China Geology 8 (2025) 843−861

China Geology

Journal homepage: http://chinageology.cgs.cn
https://www.sciencedirect.com/journal/china-geology

Geology, geochemistry and mineralization of the Taishang-Shuiwangzhuang supergiant gold deposit (>700 t Au), northwestern Jiaodong Peninsula, China: A review

Xiang-dong Liu[a, b,*], Zheng-jiang Ding[a, b,*], Zhong-yi Bao[a, b], Chun-ming Yan[a, b], Hao-cheng Yu[c], Jia-meng Fan[a, b], Tian-ci Xie[a, b], Zhi-ning Liu[a, b]

[a] *No.6 Geological Team of Shandong Provincial Bureau of Geology and Mineral Resources*, *Weihai* 264209, *China*
[b] *Deep Gold Exploration and Mining Technology Innovation Center of Ministry of Natural Resources*, *Weihai* 264209, *China*
[c] *China University of Geosciences (Beijing)*, *Beijing* 100083, *China*

ARTICLE INFO

Article history:
Received 21 December 2023
Received in revised form 16 September 2024
Accepted 21 October 2024
Available online 7 March 2025

Keywords:
Geochemistry
Mineralization
Super giant gold deposit
Ore-forming age
Ore-forming fluids
H_2O-CO_2-NaCl-type hydrothermal solutions
Crust-mantle interactions
Basic magma
Metallogenic prediction
Mineral exploration engineering
Taishang-Shuiwangzhuang
Jiaodong Peninsula

ABSTRACT

The Taishang-Shuiwangzhuang gold deposit is located in the southeastern margin of Linglong gold field in the northern part of the Zhaoping Fault metallogenic belt of the Jiaodong gold province—the world's third-largest gold metallogenic area. Major prospecting breakthroughs have been made at the depth of 600–2500 m in recent years, with cumulative proven gold resources exceeding 700 t. Based on a large number of exploration data, the main characteristics of the deposit are described in detail, and the spatial coupling relationship between ore-controlling fault and main orebodies is discussed. The main orebodies occur as regular large veins, exhibiting branching and combination, expansion and contraction, and pinch-out and reoccurrence. They extend in a gentle wave pattern along their strikes and dip directions and generally have a pitch direction of NEE and a plunge direction of NEE. As the ore-controlling fault, the Zhaoping Fault has the characteristics of wave-like fluctuation, with its dip angle presenting three steps of steep - slow transition within the depth range of 2500 m. The gold mineralization enrichment area is mainly distributed in the step parts where the fault plane changes from steeply to gently. The ore-forming age, ore-forming fluid and ore-forming material sources and the genesis of the ore deposit are analyzed based on the research results of ore deposit geochemistry. The ore-forming fluids were H_2O-CO_2-NaCl-type hydrothermal solutions with a medium-low temperature and medium-low salinity. The H-O isotopic characteristics indicate that the fluids in the early ore-forming stage were possibly formed by degassing of basic magma and that meteoric water gradually entered the ore-forming fluids in the late ore-forming stage. The S and Pb isotopes indicate that the ore-forming materials mainly originate from the lower crust and contain a small quantity of mantle-derived components. The comprehensive analysis shows that the Taishang-shuiwangzhuang gold deposit was a typical "Jiaodong type" gold deposit. The strong crust-mantle interactions, large-scale magmatism, and the material exchange arising from the transformation from the ancient lower crust to the juvenile lower crust during the Early Cretaceous provided abundant fluids and material sources for mineralization. Moreover, the detachment faults formed by the rapid magmatic uplift and the extensional tectonism created favorable temperature and pressure conditions and space for fluid accumulation and gold precipitation and mineralization.

1. Introduction

The Jiaodong Peninsula, the world's third largest gold province, holds cumulative proven gold resources of over 5500 t (Deng J et al., 2023; Song MC et al., 2023a), instrumental in establishing China as a globally leading gold producer. Despite this, China is facing an increasing gap between gold production and sales due to years of gold exploration and exploitation. The latest statistics of the China Gold Association reveal that 2023 saw gold production of 375.15 t from raw materials and gold consumption of 1089.69 t, suggesting a gap reaching up to 714.54 t. Under the context of a continuous surge in gold demand, giant mineral deposits (ore districts) have become primary exploration targets

* Corresponding author: *E-mail address*: liuxd1989@foxmail.com (Xiang-dong Liu); ytdzhj@126.com (Zheng-jiang Ding).

Literary editor: Li-qiong Jia
doi:10.31035/cg2023152
2096-5192/© 2025 China Geology Editorial Office.

(Groves DI et al., 2018), and their formation and positioning also serve as major research fronts globally in the field of geoscience (Yang LQ et al., 2019; Deng J et al., 2023).

The Taishang-Shuiwangzhuang giant gold deposit, located in the southeastern margin of the Linglong gold orefield in the northern portion of the Zhaoping fault metallogenic belt within the Jiaodong gold province (Fig. 1), has undergone shallow and deep exploration successively since its discovery in the 1960s. With the implementation of the strategy for prospecting deep deposits and the National Exploration & Development Planning, great progress has been made in the deep (600–2500 m) and peripheral prospecting of the Taishang-Shuiwangzhuang gold deposit since the beginning of the 21st century. At present, this deposit holds cumulative proven gold resources of greater than 700 t, establishing it as the largest gold deposit in the north portion of the Zhaoping fault zone. Extensive studies have been conducted on the gold deposit (Zhou FY and Li ZL, 1991, 1994; Zhao LQ et al., 2008; Bao ZY et al., 2014; Chen BH et al., 2014; Yang LQ et al., 2016; Liu GD et al., 2017, 2019; Liu GD and Li J, 2019; Li J et al., 2021; Liu XD et al., 2022a; Wang YQ et al., 2022a, 2022b), achieving certain significant insights into ore-controlling factors, alteration and mineralization characteristics, metallogenic stages, deposit geochemistry, ore-forming fluids, source of ore-forming materials, and metallogenic prediction. It is largely accepted that the gold precipitation, enrichment, and mineralization in the Taishang-Shuiwangzhuang giant gold deposit resulted from the immiscibility or boiling process of fluids (Zhou FY and Li ZL, 1991; Yang LQ et al., 2016; Li J et al., 2021). However, the source of ore-forming fluids in the deposit remains controversial, being considered to exhibit the characteristics of deep magmas (Li J et al., 2021), be closely associated with the crust (Chen BH et al., 2014), or originate from the subduction and dehydration of the paleo-Pacific slab (Yang LQ et al., 2016). Additionally, the deposit encompasses several ore blocks like Taishang, Dongfeng, and Shuiwangzhuang. However, previous studies primarily focus on a part at depths less than 600 m or a single ore block, lacking a systematic analysis of the metallogenic characteristics, orebodies' spatial occurrence patterns, and origin of the deposit in deep parts and the deposit as a whole. This makes it difficult to achieve major breakthroughs in subsequent ore prospecting. In recent years, the authors of this study have participated in the gold exploration at a depth of 2500 m in the Taishang-Shuiwangzhuang area, systematically revealing the deposit's deep characteristics. By organizing the major achievements obtained from previous shallow explorations and recent deep explorations, this study expounded on the primary characteristics of the deposit, analyzed the spatial distributions of orebodies and their deep changes, and reviewed the previous research outcomes in the geochemistry and mineralization epochs of the deposit. On this basis, this study delved into the spatial coupling relationships between faults and orebodies of the deposit, explored the sources of ore-forming materials and fluids, and proposed the genetic mode of the deposit. This study, as an exemplary case for in-depth research into the mineralization of similar gold deposits in the Jiaodong Peninsula, assists in further understanding their metallogenic regularity and formation mechanism and offers a reference for regional ore prospecting.

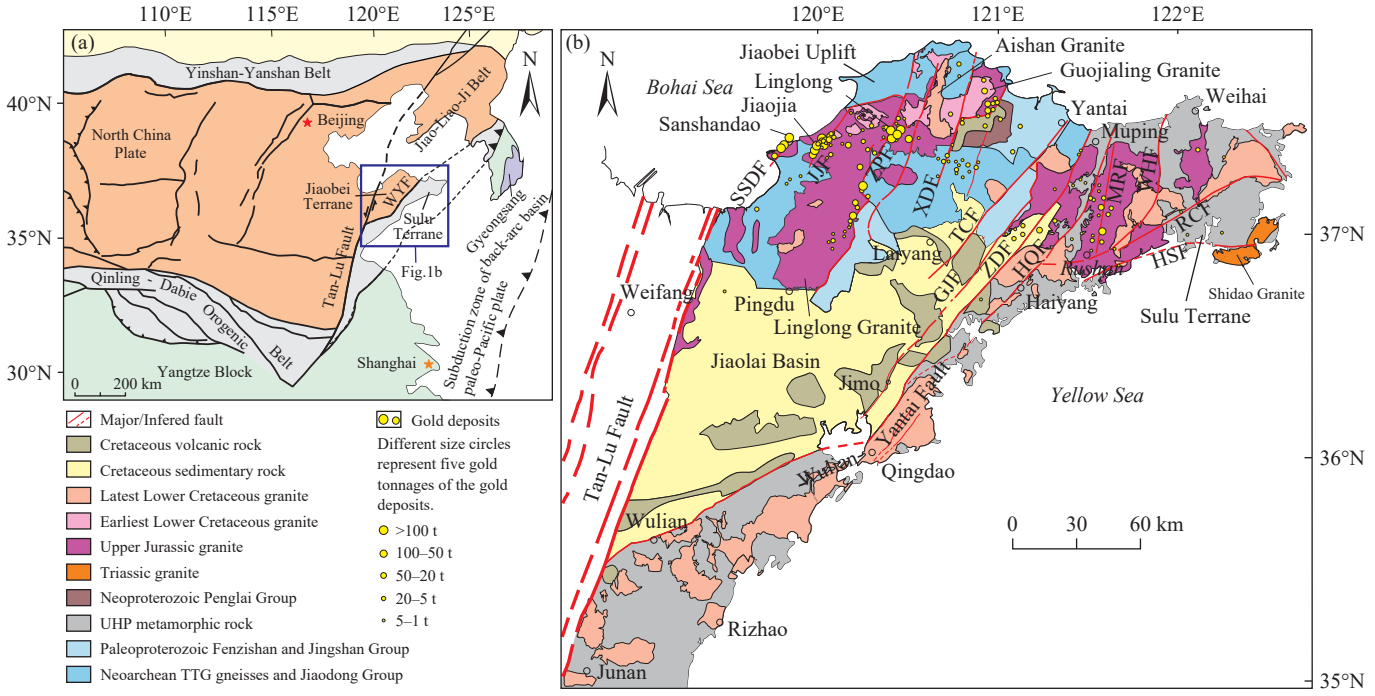

Fig. 1. a–Regional geological sketch map; b–geological map of the Jiaodong gold province showing the distribution of gold deposits in terms of size (modified from Deng J et al., 2020a, 2020b and Song MC et al., 2020). GJF–Guocheng-Jimo fault; HQF–Haiyang-Qingdao fault; HSF–Haiyang-Shidao Fault; JJF–Jiaojia fault; MRF–Muping-Rushan fault; RCF–Rongcheng fault; SSDF–Sanshandao fault; TCF–Taocun fault; WHF–Weihai fault; XDF–Xilin-Douya fault; ZDF–Zhuwu-Dianji fault; ZPF–Zhaoping fault.

2. Regional geology

The Jiaodong gold province, where the Taishang-Shuiwangzhuang gold deposit is located, experienced multi-phase tectonic superposition and composition (Deng J et al., 2023). In particular, the intense Yanshanian tectono-magmatic activity led to the Mesozoic metallogenic explosion (Mao JW et al., 1999; Zhai MG et al., 2004). The Jiaodong Peninsula is composed primarily of two tectonic units: The Jiaobei terrane within the North China Plate and the Sulu Terrane within the Qinling-Dabie-Sulu Orogen (Yang LQ et al., 2014; Deng J et al, 2020a, 2020b; Fan HR et al., 2021). The Jiaobei terrane, located in the southeastern margin of the North China plate, consists of the Jiaobei uplift in the north and the Jiaolai Basin in the south. The Sulu Terrane, situated on the northeastern margin of the Qinling-Dabie-Sulu Orogen, is dominated by the Weihai Uplift (Fig. 1). The Jiaobei Uplift primarily comprises Precambrian metamorphic basement rocks and Mesozoic intrusions, with small quantities of Paleogene-Neogene volcanic rocks and clastic sediments and Quaternary loose sediments distributed in the coastal area. The Precambrian basement is composed primarily of the amphibolites (metagabbros), biotite leptynites, and plagiogneisses of the Neoarchean Jiaodong Group; the Neoarchean tonalite-trondhjemite-granodiorite (TTG) gneisses; the marbles, schists, diopsides, and leptynites of the Paleoproterozoic Jingshan and Fenzishan groups, and the metamorphic sedimentary rocks of both the Mesoproterozoic Zhifu Group and the Neoproterozoic Penglai Group. The Jiaolai Basin is a Cretaceous continental basin composed of continental volcanic-sedimentary rocks, including the Early Cretaceous Laiyang and Qingshan groups and the Late Cretaceous - Paleocene Wangshi Group (Li SJ, 1998; Li JL et al., 2007; Ren FL et al., 2008). The Weihai Uplift, a part of the Triassic collisional orogenic belt between the North China Plate and the Yangtze Plate, consists predominantly of the ultrahigh-pressure metamorphic belts and Mesozoic intrusions. The ultrahigh-pressure metamorphic belt is composed primarily of Neoproterozoic granitic gneisses and a small quantity of Neoarchean-Paleoproterozoic metamorphic supracrustal rocks, interbedded with eclogites and mafic-ultramafic rock lenses (Ames L et al., 1996; Liu LS et al., 2018). This metamorphic belt underwent eclogite-facies ultrahigh-pressure metamorphism at 240–220 Ma (Wallis S et al., 1999). The Mesozoic intrusions are extensively distributed in the Jiaodong Peninsula, and they can be categorized into Late Triassic granites (the Shidao pluton) (Chen JF et al., 2003; Gao TS et al., 2004; Guo JH et al., 2005; Chen JZ and Jiang N, 2011), Late Jurassic granites (Linglong- and Wendeng-type granites) (Zhang J et al., 2010; Jiang N et al., 2012; Ma L et al., 2013; Yang LQ et al., 2018), granodiorites formed in the early stage of the Early Cretaceous (Guojialing-type granites; Liu Y et al., 2014; Geng K et al., 2016), and granites formed in the late stage of the Early Cretaceous (Weideshan- and Laoshan-type granites; Guo JH et al., 2005; Goss SC et al., 2010). In addition, numerous intermediate-mafic dikes are distributed in the Jiaodong Peninsula (Deng J et al., 2017; Liu XF et al., 2018). Geological structures of different ages, levels, properties, and styles overlap in the peninsula, forming a complex tectonic framework, which, however, exhibits the mutual superimposition of E-W- and NE-NNE-trending structures overall (Deng J and Wang QF, 2016). The Precambrian tectonic deformation, characterized by folds and ductile shear zones, forms nearly-E-W-trending basement morphology. The Mesozoic tectonic deformation, marked by brittle faults, primarily exhibits a NE-NNE strike, followed by nearly-EW and NW-NNW strikes, presenting a NE-NNE-trending fault pattern overall. The large-scale NE-NNE-trending fault structures in the Taishang-Shuiwangzhuang gold deposit include the Sanshandao, Jiaojia, Zhaoping, Xilin-Douya, Mouping-Jimo, and Mouping-Rushan fault zones from west to east. These fault zones govern more than 90% of the proven gold resources in the Jiaodong Peninsula (Deng J and Wang QF, 2016; Deng J et al., 2019). The nearly-EW-trending structures principally include the nearly-EW-trending folds along the axial direction in the Precambrian metamorphic basement and their associated nearly-EW-trending fault structures, which jointly form an EW-trending fold-fault belt (Deng J et al., 2019). The NW-NWW-trending structures, relatively small and largely distributed in the northwest Jiaodong Peninsula, are generally post-mineralization faults (Deng J et al., 2019).

3. Ore deposit geology

3.1. General geology

The Taishang-Shuiwangzhuang gold deposit lies on the southeastern margin of the Linglong gold orefield in the northern Zhaoping fault zone, with rock suites composed primarily of Mesozoic magmatic rocks, along with small quantities of Neoarchean TTG gneisses (Bao ZY et al., 2014; Liu GD et al., 2017, 2019; Liu XD et al., 2022a). Roughly bounded by the Zhaoping fault zone, the Mesozoic magmatic rocks in the footwall predominantly comprise Late Jurassic Linglong-type granites hosting NNE-directed diorite porphyrite and lamprophyre veins, and those in the hanging wall are identified as Late Jurassic Luanjiahe-type granites, with Guojialing-type granites formed in the early stage of the Early Cretaceous intruded into both types of granites. The Neoarchean TTG gneisses, appearing as xenoliths, are primarily distributed in Late Jurassic Luanjiahe-type granites. NNE- and NE-trending fault structures are found within the deposit, primarily including the Zhaoping, Linglong, and Luanjiahe faults. The Zhaoping fault, acting as the dominant ore-controlling structure, branches into two at the Jiuqu Village: The NE-trending Potouqing fault and the NNE-trending Jiuqu-Jiangjia fault. The Potouqing fault exhibits an overall strike of 60°, a dip direction of SE, and dip angles

generally ranging from 18° to 45°, with the major fault plane marked by fault gouge developing in this fault. The Jiuqu-Jiangjia Fault manifests an overall strike of 25°, a dip direction of SEE, and relatively high dip angles, which reach up to a maximum of 51° near the surface and gradually range from 10° to 36° toward the depth. Major fault plane marked by fault gouge is also found in this fault. Additionally, NE- and NNE-trending secondary faults are extensively distributed in the footwall of the Zhaoping Fault, forming a Linglong-type broom-like structure that spreads southwestward and converges northeastward (Li SX et al., 2007), which governs the occurrence and distribution of gold orebodies (veins) within the deposit (Fig. 2). Extensive hydrothermal alterations are found along fault structures in the deposit, characterized by large-scale alteration zones and complete alteration types, which roughly mirror those of similar gold deposits (Liu XD et al., 2019, 2022b; Song MC et al., 2021) and are dominated by K-feldspar alteration, silicification, sericitization, carbonation, and chloritization (Zhao LQ et al., 2008; Yang LQ et al., 2016).

3.2. Characteristics of orebodies

Over 500 gold orebodies have been delineated within the Taishang-Shuiwangzhuang gold deposit. A systematical analysis of their occurrence locations and geological characteristics reveals that the main orebodies in various ore blocks all occur within the beresitized cataclasite zones or beresitized, granitic cataclasite zones in the footwall of major fault planes. These orebodies can be connected both in the planar view and profile, generally pitching and dipping toward NEE (Fig. 3).

The orebodies within the deposit occur as regular large veins, exhibiting branching and combination, expansion and contraction, and pinch-out and reoccurrence (Fig. 4). They extend in a gentle wave pattern along their strikes and dip directions. Their strikes are roughly consistent with those of the major fault planes. The orebodies controled by the Potouqing fault exhibit strikes ranging from 20° to 80° (average: 56°), a dip direction of SE, and dip angles generally varying from 25° to 50° (average: about 40°). The orebodies under the control of the Jiuqu-Jiangjia fault manifest an average strike of 20°, a dip direction of SE, and dip angles generally ranging from 15° to 35°. Overall, the dip angles of the orebodies within the deposit display a downward trend from shallow to deep parts. They are generally about 40° and up to a maximum of 50° in deep parts with elevations less than −500 m and vary primarily between 20° and 40° in shallower parts. They show the maximum drilling-controlled length along their strikes of 5860 m (elevation: −1050 m), the maximum length along their dip directions of 3200 m (exploration line: No. 43), and single-drilling-controlled thickness generally ranging from 3.00 m to 20.00 m, up to a maximum of 72.35 m, and an average thickness of 11.73 m. Their gold grades commonly fall within a range of 2.00–10.00 g/t, with a maximum of 100.70 g/t and an average of 3.14 g/t.

3.3. Characteristics of ores and gold minerals

There are mainly three types of ores in the Taishang-Shuiwangzhuang gold deposit: Fine-grained disseminated - veinlet beresitized cataclasite (Figs. 5a, d, g), disseminated-veinlet-stockwork beresitized granitic cataclasites (Figs. 5b, e, h), and veinlet-stockwork beresitized granite (Figs. 5c, f, i),

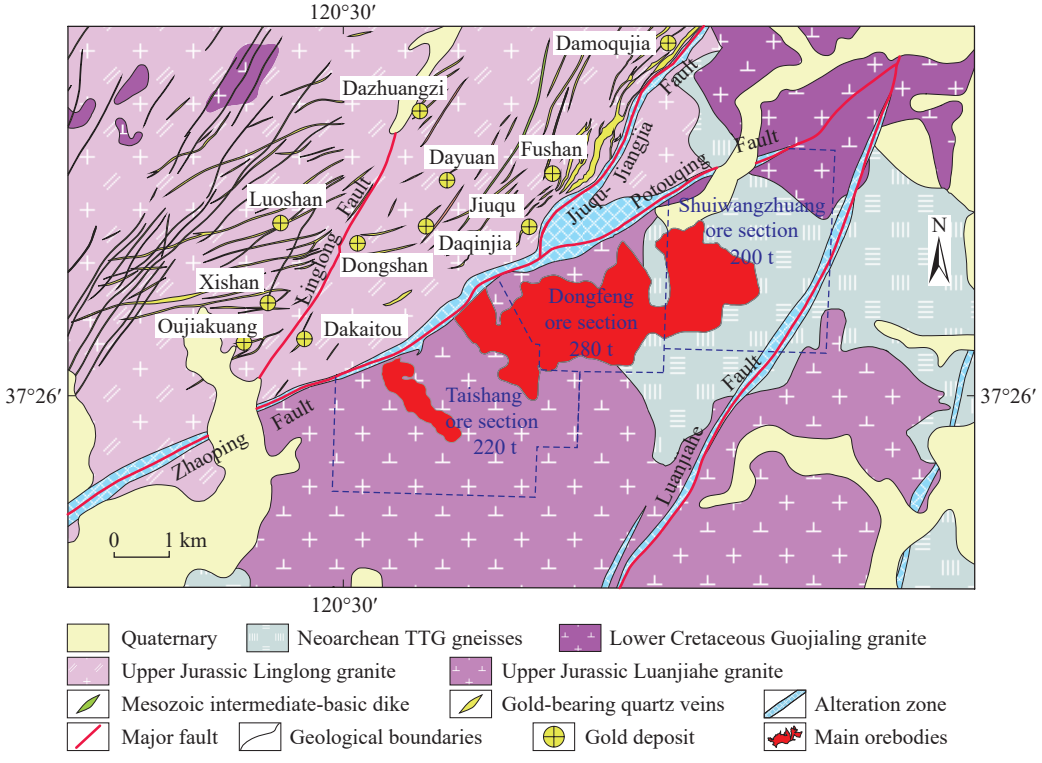

Fig. 2. Geological map of the Taishang-Shuiwangzhuang gold deposit (modified from Yang LQ et al., 2016 and Liu XD et al., 2022a).

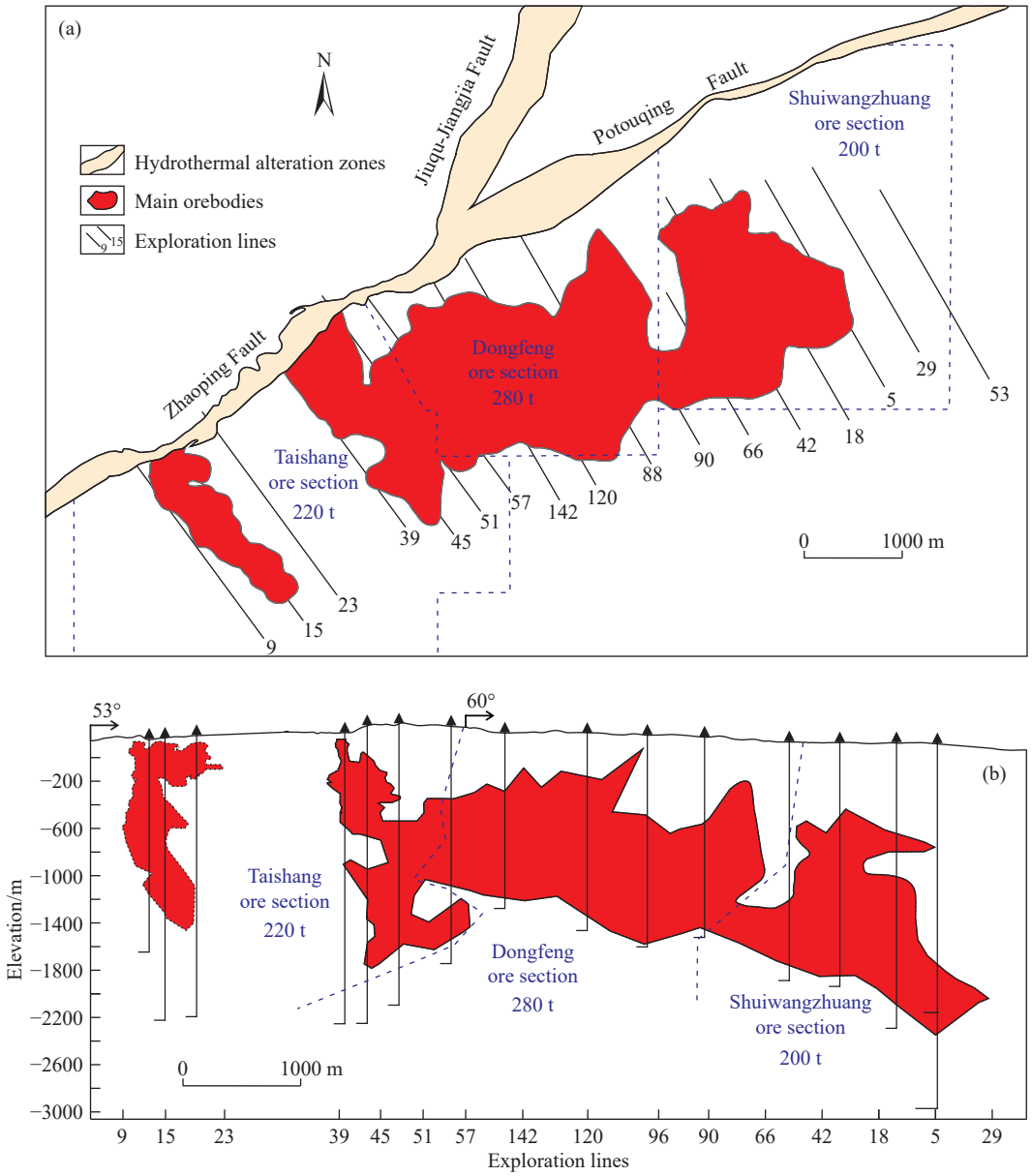

Fig. 3. a–Horizontal projection; b–vertical projection of the primary orebodies in the Taishang-Shuiwangzhuang gold deposit.

with the former two types predominating. The ores of the first, second, and third types are primarily distributed in the beresitized cataclasite zones in the footwall of major fracture planes, beresitized granitic cataclasite zones, and beresitized granite zones, respectively. Metallic minerals in the ores principally include electrum, native gold, native silver, pyrite, chalcopyrite, galena, sphalerite, and pyrrhotite. Nonmetallic minerals in the ores primarily encompass quartz, sericite, and feldspar. Pyrite, the most predominant metallic mineral and a major gold-bearing mineral in the ores, exhibits content ranging from 2% to 5% and up to a maximum of above 30%. The ore textures are dominated by granular textures, followed by cataclastic, interstitial, etching, poikilitic, and opaque textures. The ore structures are dominated by disseminated and veinlet disseminated structures, followed by spotted, stockwork, and staggered structures. Gold minerals in the ores are dominated by electrum (59%), followed by native gold (40%). The gold fineness of the ores varies from 508‰ to 955‰ (average: 770‰), concentrated within a range of 600‰–900‰. The gold is generally fine-grained (0.037–0.01 mm; 28.41%) and micro-grained (below 0.01 mm; 62.27%). It is predominantly granular in shape (78.92%) and primarily occurs as interstitial gold (56.11%; Fig. 5i), followed by inclusion gold (34.87%; Fig. 5g), alongside trace amounts of fissure gold (9.02%; Fig. 5h).

The beneficial components in the ores are mostly gold, with gold content ranging from 0.80 g/t to 248.00 g/t, averaging 3.93 g/t. Among the associated beneficial components, silver and sulfur meet their evaluation criteria, with average contents of 6.30 g/t and 2.27%, respectively.

3.4. Ore-forming stages

The Taishang-Shuiwangzhuang gold deposit is found to have experienced four metallogenic stages according to its mineral assemblages, textures, and structures, as well as the

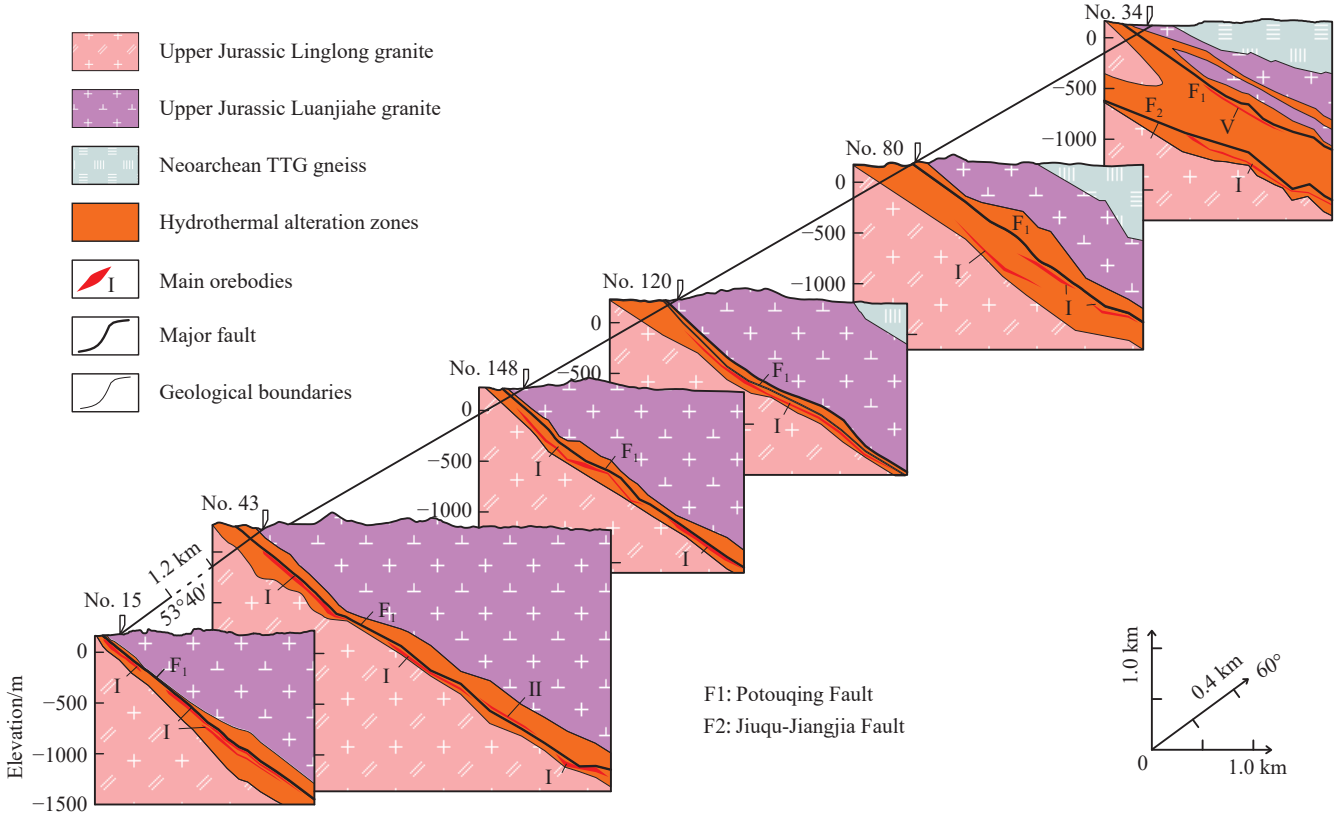

Fig. 4. Combined cross-sections of the Taishang-Shuiwangzhuang gold deposit.

crosscutting relationships of hydrothermal veins (Table 1; Guo LN, 2016; Yang LQ et al., 2016). Stage I is the pyrite-quartz-sericite stage. This stage features white hydrothermal veins consisting primarily of quartz and small quantities of pyrites and sericites. Stage II is the gold-quartz-pyrite stage. This stage is characterized by grayish-yellow, gold-bearing hydrothermal mineralized veins, which are distributed as veinlets in fractured zones. The mineralized veins of this stage consist primarily of pyrites and small quantities of quartz, sericites, native gold, and electrum. Stage III is the gold-quartz-polymetallic sulfide stage. The mineralized veins of gold-bearing hydrothermal solutions of this stage are grayish-yellow, distributed as veinlets and micro-veins in fractured zones. These veins predominantly comprise quartz, pyrites, chalcopyrite, galena, and sphalerite, with small amounts of electrum and kustelite discovered. Stage IV is the quartz-carbonate stage. The hydrothermal veins of this stage, distributed as veins and veinlets in fractured zones, consist primarily of calcites and a small amount of quartz. From early to late metallogenic stages, mineralization intensifies and then weakens, and the mineral assemblages became complex and then simple. They transitioned from the predominance of pyrites to the coexistence of galena, sphalerite, and pyrites, culminating in the occurrence of carbonate veins. Gold was primarily precipitated in metallogenic stages II and III.

4. Ore deposit geochemistry

4.1. Fluid inclusions

The fluid inclusions in the Taishang-Shuiwangzhuang gold deposit generally exhibit small diameters ranging from 2 μm to 15 μm and various morphologies like oval, elongated, and negative crystal shapes. Three types of fluid inclusions are found in the deposit: H_2O-CO_2, H_2O solution, and pure CO_2 (Fig. 6), with the H_2O-CO_2 type predominating. They are three-phase (L_{H2O}+L_{CO2}+V_{CO2}) or two-phase (L_{H2O}+L_{CO2}/V_{CO2}) at room temperature (25°C), presenting a relatively regular elliptical shape, along with a negative crystal shape and partially. Their grain sizes vary from approximately 3 mm to 20 mm. Based on the volume fraction of the CO_2 phase in the total volume, the H_2O-CO_2 inclusions can be categorized into H_2O-rich (L_{CO2}±V_{CO2} < 50%) and CO_2-rich (L_{CO2}±V_{CO2} > 50%) inclusions, which exhibit L_{CO2}±V_{CO2} volume fractions varying from 3% to 40% (primarily 5%–30%) and from 50% to 90%, respectively. The H_2O solution inclusions are two-phase (L_{H2O}+V_{H2O}) at room temperature, with gas to liquid ratios generally ranging from 10% to 60% (maximum: up to 90%) and sizes generally less than 5 mm. The pure CO_2 inclusions are two-phase or single-phase (L_{CO2}±V_{CO2}) at room temperature, with sizes of 3–5 mm.

For the H_2O-CO_2 inclusions, their vapor-phase components primarily include CO_2 and a small amount of CH_4, with no H_2S, SO_2, N_2, and CO being detected, and their liquid-phase components are dominated by H_2O. The pure CO_2 inclusions comprise primarily CO_2, with a small amount of CH_4 being identified (Yang LQ et al., 2016).

The fluid inclusions formed in metallogenic stage I are dominated by the H_2O-CO_2 type. The solid-phase CO_2 in the H_2O-CO_2 inclusions exhibit melting temperatures ($T_{m\text{-}CO2}$)

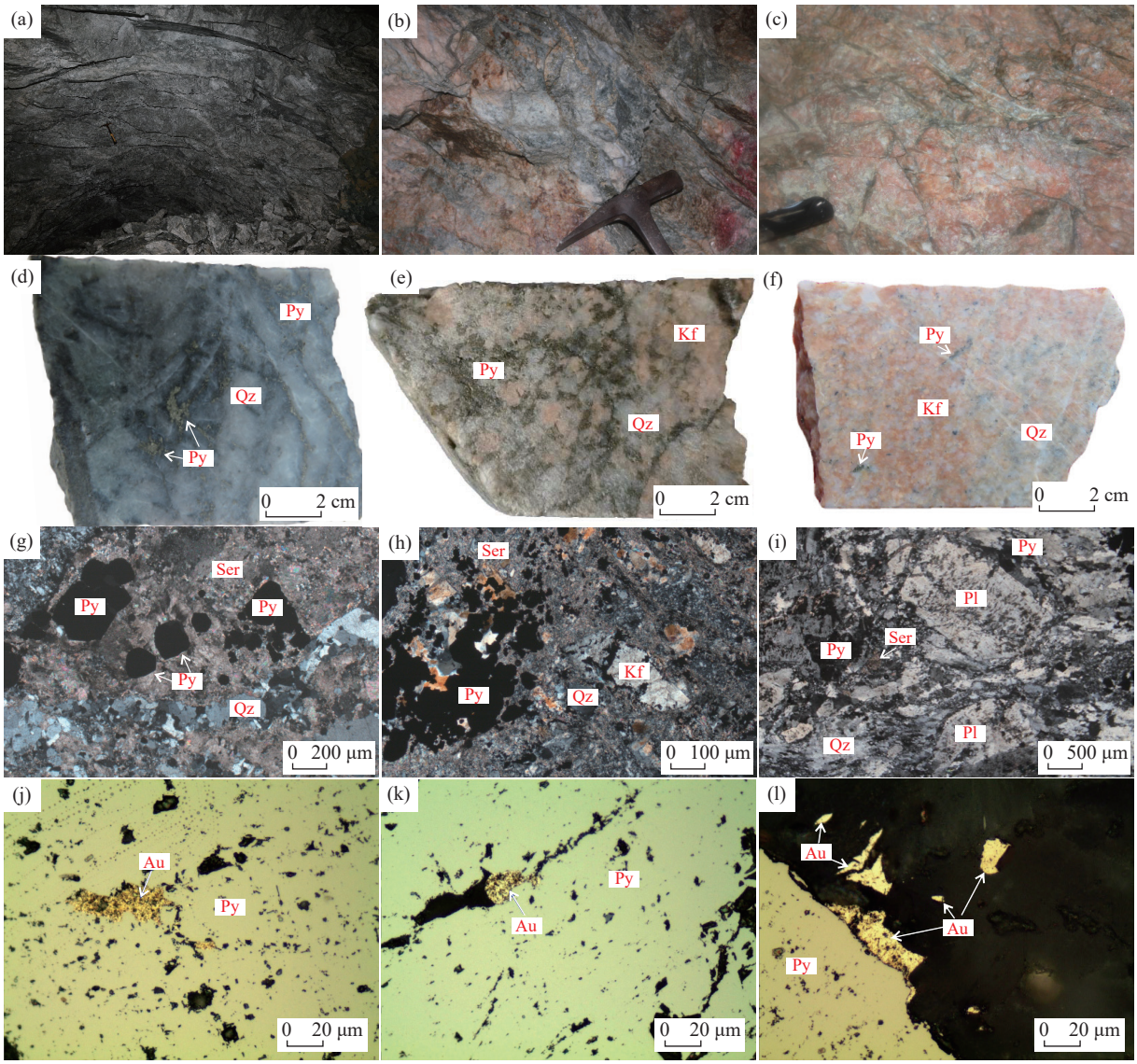

Fig. 5. Photos and photomicrographs of primary gold ore types and gold minerals in the Taishang-Shuiwangzhuang gold deposit. a, d, g–Disseminated and veinlet-stockwork beresitized cataclasite type; b, e, h–veinlet-stockwork beresitized granitic cataclasite type; c, f, i–veinlet-stockwork beresitized granite type. Au–gold minerals; Kf–K-feldspar; Pl– plagioclase; Py–pyrite; Qz–quartz; Ser–sericite.

Table 1. Paragenetic sequence of primary minerals in the Taishang-Shuiwangzhuang gold deposit (after Yang LQ et al., 2016).

Stage / Mineral	Stage I	Stage II	Stage III	Stage IV
Quartz				
Sericite				
Pyrite				
Native gold				
Electrum				
Chalcopyrite				
Pyrrhotite				
Galena				
Sphalerite				
Telluride				
Calcite				

ranging from −57.3°C to −56.6°C, slightly lower than the triple point temperature of pure CO_2 (−56.6°C). This finding indicates that, besides CO_2, the CO_2 phase in the H_2O-CO_2 inclusions may contain a trace amount of CH_4 or other vapor-phase components. Furthermore, the H_2O-CO_2 inclusions exhibit total homogenization temperatures ($T_{h\text{-}TOT}$) varying from 276°C to 336°C and salinity from 1.40 wt.% NaCl eqv to 11.70 wt.% NaCl eqv. The inclusions formed in metallogenic stage II include the coexisting H_2O-CO_2, pure CO_2, and H_2O solution types, with $T_{h\text{-}TOT}$ values ranging from 187°C to 317°C and salinity from 0.20 wt.% NaCl eqv to 10.80 wt.% NaCl eqv. Similar to stage II, metallogenic stage III also exhibits coexisting H_2O-CO_2, pure CO_2, and H_2O solution inclusions, except that the proportion of the H_2O solution inclusions increases significantly. The inclusions of this stage exhibit $T_{h\text{-}TOT}$ values varying from 125°C to 315°C and salinity from 3.00 wt.% to 10.80 wt.%. The inclusions formed in metallogenic stage IV principally include H_2O solution inclusions, followed by a small quantity of H_2O-CO_2 fluid inclusions, with $T_{h\text{-}TOT}$ values primarily ranging from

117°C to 236°C and salinity from 0.50 wt.% NaCl eqv to 8.50 wt.% NaCl eqv (Table 2).

4.2. H-O isotopes

The H-O isotopes in the Taishang-Shuiwangzhuang gold deposit were tested at the Beijing Research Institute of Uranium Geology. The H isotopes were analyzed as follows: (1) A Thermo Flash elemental analyzer was flushed with high-purity (99.999%) helium to expel air and reduce the background values of H_2 and CO; (2) quartz was heated to about 1380°C using the elemental analyzer to release water; (3) the released water flowed through a ceramic tube bearing glassy carbon. In the tube, the water reacted with excess carbon to generate H_2 gas, which was then introduced into a MAT-253 mass spectrometer for tests. The O isotope test process is detailed below: (1) Quartz, after being pulverized to 200 mesh, reacted with BrF_5 at 500°C–600°C for 14 h to release O_2 and impurities; (2) with platinum (Pt) as the catalyst, the generated O_2 further reacted with graphite under a constant temperature of 700°C to generate CO_2, which was then tested using a MAT-253 mass spectrometer. The H-O isotopes were tested based on the standard mean ocean water (SMOW), yielding $\delta D_{V\text{-}SMOW}$ and $\delta^{18}O_{V\text{-}SMOW}$ values, with analytical accuracies of ±1‰ and ±0.2‰, respectively. The analytical results are shown in Table 3.

For the Taishang-Shuiwangzhuang gold deposit, the fluids

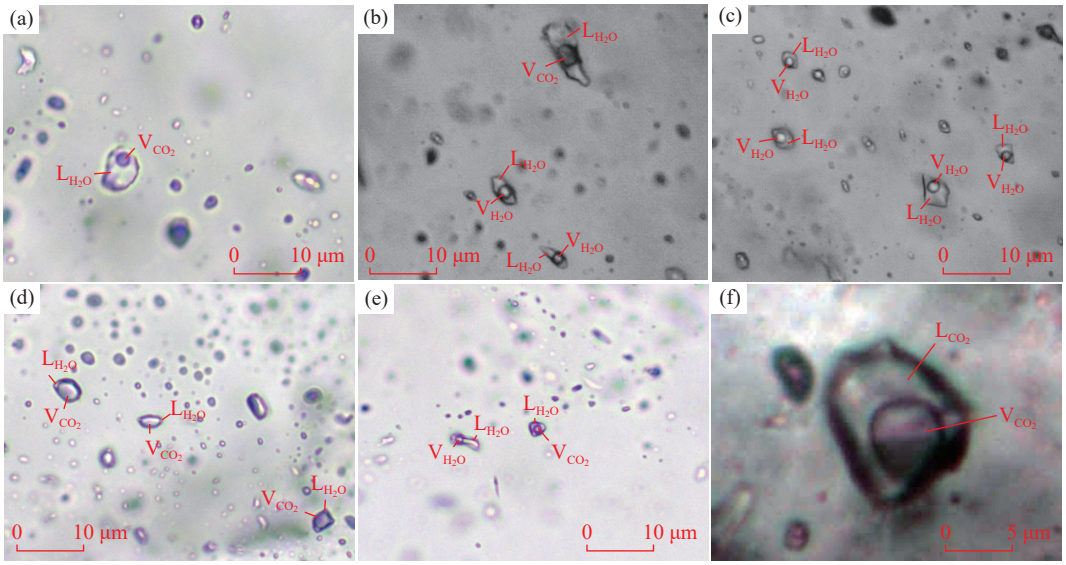

Fig. 6. Photomicrographs of typical fluid inclusions in the Taishang-Shuiwangzhuang gold deposit. a–Aqueous-carbonic type (L_{H2O}+V_{CO2}); b–aqueous type (L_{H2O}+ V_{H2O}) and aqueous-carbonic type (L_{H2O}+V_{CO2}); c–aqueous type (L_{H2O}+ V_{H2O}); d–aqueous-carbonic type (L_{H2O}+V_{CO2}); e–aqueous type (L_{H2O}+ V_{H2O}) and aqueous-carbonic type (L_{H2O}+V_{CO2}); f–pure carbonic type (L_{CO2}+ V_{CO2}).

Table 2. Summary of microthermometric data from fluid inclusions trapped in quartz in four metallogenic stages in the Taishang-Shuaiwangzhuang gold deposit.

Ore block	Stage	Fluid inclusion type	$T_{m\text{-}CO2}$/°C	$T_{m\text{-}cla}$/°C	$T_{h\text{-}CO2}$/°C	$T_{m\text{-}ice}$/°C	$T_{h\text{-}TOT}$/°C	Salinity/(wt.% NaCl eqv)	References
Taishang	Ⅰ	H_2O-CO_2-NaCl	−57.3 – −56.6	6.2–9.3	24.0–29.9		285–336	1.40–7.10	Yang LQ et al., 2016
	Ⅱ	H_2O-CO_2-NaCl	−60.2 – −56.6	5.0–9.8	18.8–29.3		215–314	0.40–9.10	
		H_2O-CO_2-NaCl	−59.3 – −57.5	6.1–9.9	17.8–29.4		256–317	0.20–7.30	
	Ⅲ	H_2O-CO_2-NaCl	−59.4 – −56.9	5.8–8.5	17.2–26.7		212–298	3.00–7.80	
		H_2O-CO_2-NaCl	−57.9 – −57.8	7.3–7.7	20.5–22.6		252–315	4.50–5.20	
	Ⅳ	H_2O-CO_2-NaCl	−56.9 – −56.6	6.1–9.5	18.4–30.1		158–236	1.00–7.30	
Dongfeng	Ⅰ	H_2O-CO_2-NaCl				/	276–341	2.80–11.70	Wan D, 2014; Chen YM et al., 2016
	Ⅱ	H_2O-CO_2-NaCl	−57.4 – −56.6	6.5–7.8	28.1–31.0		219–310	3.30–10.80	
		H_2O- NaCl				/	171–300	6.50–10.50	
	Ⅲ	H_2O-CO_2-NaCl	/	/	/		248–310	3.30–10.80	
	Ⅳ	H_2O- NaCl				/	117–219	0.50–8.50	
Shuaiwangzhuang	Ⅱ	H_2O-CO_2	/	/	/		210–234	5.10–5.90	Wan D, 2014
		H_2O-CO_2-NaCl				/	187–201	9.50–10.80	
	Ⅲ	H_2O- NaCl				/	125–159	4.00–4.90	
		H_2O-CO_2-$NaCl_2$	/	/	/		216–229	5.54–6.93	
	Ⅳ	H_2O- NaCl				/	136–146	4.01–4.63	

Notes: $T_{m\text{-}CO2}$ is the melting temperature of solid CO_2 phase; $T_{m\text{-}cla}$ is the melting temperature of clathrates; $T_{h\text{-}CO2}$ is the homogenization temperature of CO_2 phase; $T_{m\text{-}ice}$ is the temperature of final ice melting; $T_{h\text{-}TOT}$ is the final homogenization temperature; wt. % NaCl eqv is the weight percent NaCl equivalent.

Table 3. Hydrogen and oxygen isotopic compositions of four metallogenic stages in the Taishang-Shuiwangzhuang gold deposit.

Ore section	Sample	Location	Stage	Mineral	δD_{SMOW} /‰	$\delta^{18}O_{SMOW}$ /‰	$\delta^{18}O_{H2O}$ /‰	T /°C	References
Taishang	LN-B3	51ZK1, 1442 m	II	Quartz	−96.1	9.2	1.6	280	This paper
	LN26-B2	CM5, −920 m	III	Quartz	−90.1	7.6	−0.9	260	
Dongfeng	DF171-B3	CM108, −380 m	II	Quartz	−92.4	12.7	5.1	280	
Shuiwangzhuang	LJZ-B3	26ZKL1, 1336 m	II	Quartz	−87.4	12.6	5.0	280	
	LJZ-B1	1KL3, 1667 m	III	Quartz	−90.8	8.8	0.3	260	
	SWZ42-B3	42ZKC12, 1584 m	II	Quartz	−92.4	10.8	3.2	280	
	SWZ42-B4	42ZKC10, 1688 m	II	Quartz	−84.7	11.1	3.5	280	
	SWZ26-B1	26ZKC1, 1285 m	II	Quartz	−76.2	10.2	2.6	280	
	SWZ26-B3	26ZKC1, 1824 m	III	Quartz	−89.1	9.4	0.9	260	
	SWZ26-B2	26ZKC4, 1518 m	III	Quartz	−82.3	10	1.5	260	
	SWZ26-B5	26ZKC4, 1765 m	III	Quartz	−91.9	10.8	2.3	260	
Taishang	/	/	I	Quartz	−99 – −78; −88 (*n*=13)	7.3–15.7; 11.3 (*n*=13)	0.6–9.0; 4.6 (*n*=13)	306	Zhang LG et al, 1995a; Yang LQ et al., 2016
	/	/	I	Sericite	−80 – −76; −78 (*n*=4)	/	/	306	
	/	/	II	Quartz	−90 – −74; −84 (*n*=13)	9.2–13.8; 11.7 (*n*=13)	1.6–6.2; 4.0 (*n*=13)	280	Zhang LG et al, 1995a; Yang LQ et al., 2016
	/	/	II	Sericite	−94 – −80; −86 (*n*=4)	/	/	280	
	/	/	III	Quartz	−88 – −80; −85 (*n*=3)	11.2–12.0; 11.7 (*n*=3)	2.7–3.5; 3.2 (*n*=3)	260	Yang LQ et al., 2016
	/	/	IV	Quartz	−91 – −84; −88 (*n*=2)	13.2–15.4; 14.3 (*n*=2)	1.5–3.7; 2.6 (*n*=2)	200	Zhang LG et al, 1995a; Yang LQ et al., 2016
Shuiwangzhuang	/	−1479 – −1900 m	II /III	Quartz	−92 – −83; −88 (*n*=7)	9.5–12.6; 11.3 (*n*=7)	1.0–4.1; 2.8 (*n*=7)	260	Li J et al., 2021

Notes: $\delta^{18}O_{water}$ (‰) is calculated based on $\delta^{18}O_{SMOW}$ (‰; quartz) using equation $\delta^{18}O_{water} = \delta^{18}O_{SMOW} - 3.38 \times 10^6 T^{-2} + 3.40$ (Clayton RN et al., 1972)

in metallogenic stage I exhibit $\delta D_{SMOW\text{-}water}$ values ranging from −99‰ to −78‰ (average: −88‰; n = 13) and $\delta^{18}O_{SMOW\text{-}water}$ values from 0.6‰ to 9.0‰ (average: 4.6‰; n = 13). The hydrothermal quartz of metallogenic stage II manifests $\delta D_{SMOW\text{-}water}$ values varying from −96.1‰ to −74.0‰ (average: −85.4‰; n = 19) and $\delta^{18}O_{SMOW\text{-}water}$ values from 1.6‰ to 6.2‰ (average: 3.8‰; n = 19). The hydrothermal quartz of metallogenic stage III displays $\delta D_{SMOW\text{-}water}$ values fluctuating from −91.9‰ to −80.0‰ (average: −87.4‰; n = 8) and $\delta^{18}O_{SMOW\text{-}water}$ values from −0.9‰ to 3.5‰ (average: 1.7‰; n = 8). The hydrothermal quartz of metallogenic stage IV exhibits $\delta D_{SMOW\text{-}water}$ values ranging from −91‰ to −84‰ (average: −87.5‰; n = 2) and $\delta^{18}O_{SMOW\text{-}water}$ values from 1.5‰ to 3.7‰ (average: 2.6‰; n = 2). Additionally, the hydrothermal sericites of metallogenic stage I display $\delta D_{SMOW\text{-}sericite}$ values vary between −80‰ and −76‰ (average: −78‰; n = 4), while those of metallogenic stage II exhibit $\delta D_{SMOW\text{-}sericite}$ ranging from −94‰ to −80‰ (average: −86‰; n = 4).

4.3. S isotopes

S isotope tests were also implemented at the Beijing Research Institute of Uranium Geology. The test process is as follows: (1) Pyrite, pulverized to below 200 mesh, reacted with cuprous oxide under a temperature of 980°C and the vacuum pressure of 2×10^{-2} Pa to generate SO_2; (2) the generated SO_2 was tested using a Delta V mass spectrometer. S isotopes were tested based on the canyon diablo troilite (CDT) standard, yielding $\delta^{34}S_{V\text{-}CDT}$, with an analytical accuracy of ±0.2‰.

The Taishang-Shuiwangzhuang gold deposit exhibits $\delta^{34}S_{CDT}$ values ranging from 4.5‰ to 8.5‰ (Table 4), with a range of 4.0‰ and an average of 7.0‰ (n = 53). Specifically, the $\delta^{34}S_{CDT}$ values of metallogenic stage I vary from 4.5‰ to 7.4‰, with a range of 2.9‰ and an average of 6.4‰ (n = 6); those of metallogenic stage II from 5.7‰ to 8.0‰, with a range of 2.3‰ and an average of 6.8‰ (n = 19); and those of metallogenic stage III from 5.8‰ to 7.9‰, with a range of 2.1‰ and an average of 7.0‰ (n = 10). Additionally, metallogenic stage IV displays a $\delta^{34}S_{CDT}$ value of 6.8‰ (n = 1).

4.4. Pb isotopes

The Pb isotopes of the Taishang-Shuiwangzhuang gold deposit vary in a small range and exhibit a relatively stable composition (Table 5). They display $^{206}Pb/^{204}Pb$ values ranging from 17.4979 to 17.7260, with an average of 17.5918 (n = 16), $^{207}Pb/^{204}Pb$ values from 15.4860 to 15.6650, with an average of 15.5730 (n = 16), and $^{208}Pb/^{204}Pb$ values from 37.9950 to 38.5330, with an average of 38.2826 (n = 16).

5. Discussion

5.1. Spatial coupling relationship between ore-controlling faults and orebodies

To analyze the deep characteristics of the ore-controlling Zhaoping fault zone and its spatial relationship with orebodies in detail, this study established a three-dimensional geological

Table 4. Sulfur isotopic compositions of four metallogenic stages in the Taishang-Shuiwangzhuang gold deposit.

Ore section	Sample	Location	Stage	Mineral	$\delta^{34}S$	References
Taishang	LN-B3	51ZK1, 1442 m	II	Pyrite	6.6	This paper
	LN26-B2	CM5, −920 m	III	Pyrite	5.8	
Dongfeng	DF171-B3	CM108, −380 m	II	Pyrite	6.0	
Shuiwangzhuagn	LJZ-B3	26ZKL1, 1336 m	II	Pyrite	7.3	
	LJZ-B1	1KL3, 1667 m	III	Pyrite	6.8	
	SWZ42-B3	42ZKC12, 1584 m	II	Pyrite	6.5	
	SWZ42-B4	42ZKC10, 1688 m	II	Pyrite	7.2	
	SWZ26-B1	26ZKC1, 1285 m	II	Pyrite	6.4	
	SWZ26-B3	26ZKC1, 1824 m	III	Pyrite	6.3	
	SWZ26-B2	26ZKC4, 1518 m	III	Pyrite	6.9	
	SWZ26-B5	26ZKC4, 1765 m	III	Pyrite	6.9	
Taishang	/	/	I	Pyrite	4.5–7.4; 6.4 (*n*=6)	Yang LQ et al., 2016
	/	/	II	Pyrite	5.7–8.0; 6.8 (*n*=13)	
	/	/	III	Pyrite	6.4–7.9; 7.4 (*n*=5)	
	/	/	IV	Pyrite	6.8 (*n*=1)	
	/	/	/	Pyrite	7.0–8.3; 7.8 (*n*=5)	Hou ML et al., 2006
Dongfeng	/	/	/	Pyrite	5.8–7.0; 6.6 (*n*=5)	Chen YM et al., 2016
Shuiwangzhuang	/	−1479 – −1900 m	/	Pyrite	7.0–8.5; 7.7 (*n*=7)	Li J et al, 2021

Table 5. Lead isotopic compositions of the Taishang-Shuiwangzhuang gold deposit.

Ore section	Mineral	$^{206}Pb/^{204}Pb$	$^{207}Pb/^{204}Pb$	$^{208}Pb/^{204}Pb$	References
Taishang	Galena	17.5270–17.7260; 17.6105 (*n*=4)	15.4860–15.6650; 15.5552 (*n*=4)	37.9950–38.5330; 38.2067 (*n*=4)	①
	Pyrite	17.5480–17.6660; 17.6070 (*n*=2)	15.5770–15.6060; 15.5915 (*n*=2)	38.3110–38.3490; 38.3300 (*n*=2)	Wang YW et al., 1988
	Pyrite	17.4979–17.6627; 17.6006 (*n*=5)	15.5581–15.5950; 15.5738 (*n*=5)	38.2481–38.3849; 38.3100 (*n*=5)	Hou ML et al., 2006
	Pyrite	17.5120–17.6900; 17.5777 (*n*=5)	15.5230–15.6450; 15.5863 (*n*=5)	38.1090–38.5210; 38.3186 (*n*=5)	Guo LN, 2016

Notes: ① Shandong Provincial No.6 Exploration Institute of Geology and Mineral Resources, 1992. Intermediate geological exploration report of the Taishang ore block in the Taishang gold deposit in Zhaoyuan City, Shandong Province.

model for the Taishang-Shuiwangzhuang gold deposit at depths ranging from 0 m to 2500 m based on borehole data (Wang YQ et al., 2022a, b). Then, using information about the major fracture plane of the Zhaoping fault extracted from the 3D geological model, this study plotted the changes in the fault slope, as shown in Fig. 7a. According to this figure, the dip angle of the ore-controlling fault exhibits significant wavy fluctuations characterized by three sections of high-to-low transitions along the fault's plunge direction. The changes in the attitude of the Zhaoping fault resemble those of the Sanshandao and Jiaojia faults (Song MC et al., 2012, 2021, 2023b; Liu XD et al., 2022b), indicating that the three primary ore-controlling faults in the Jiaodong Peninsula (Sanshandao, Jiaojia, and Zhaoping faults) share consistent morphological characteristics. Therefore, these faults should belong to the same fault system formed under a unified dynamic setting (Song MC et al., 2022).

To analyze the spatial coupling relationships between faults and orebodies, this study plotted the thickness × grade values of primary orebodies, as shown in Fig. 7b. Three mineralization enrichment areas with high thickness × grade values are identified, exhibiting an alternating distribution with weakly mineralized zones (low thickness × grade values). Moreover, these mineralization enrichment areas are distributed in a beaded pattern along the plunge directions of the orebodies.

The comparison between the mineralization enrichment areas and the major fracture plane of the Zhaoping fault reveals that the ore-controlling fault exhibits dip angles varying from 5° to 55°, averaging at 30° and concentrated between 20° and 35° (Fig. 7c). The comparison also discloses that the mineralization enrichment areas lie in the steep-to-gentle transition parts of the fault (Figs. 7a, b), primarily occurring at positions with low dip angles (especially between 10° and 35°; Figs. 7a, b). This finding indicates that the gold mineralization enrichment areas are mainly distributed in the transition parts of the fault dip angle and relatively gentle steps.

The aforementioned plunge regularity of orebodies is widespread in similar gold deposits within the Jiaodong Peninsula (Song MC et al., 2012, 2022, 2023b). The formation of this pattern is associated with variations in fluid pressure caused by changes in fault dip angles. When fluids migrated toward gently dipping sections of a fault after flowing through its steep-to-gentle transition sections, the fluid pressure sharply decreased. Then, the fluids began to flow in a nearly horizontal direction at a low flow velocity. All these created favorable conditions for fluid unloading and gold precipitation. On the other hand, the plunge of gold orebodies is jointly governed by the transitions of a fault's attitude along its strike and dip direction (Song MC et al., 2022). The plunge regularity of orebodies is significant for deep prospecting, having found application in the deep prospecting of the Taishang-Shuiwangzhuang gold deposit, as

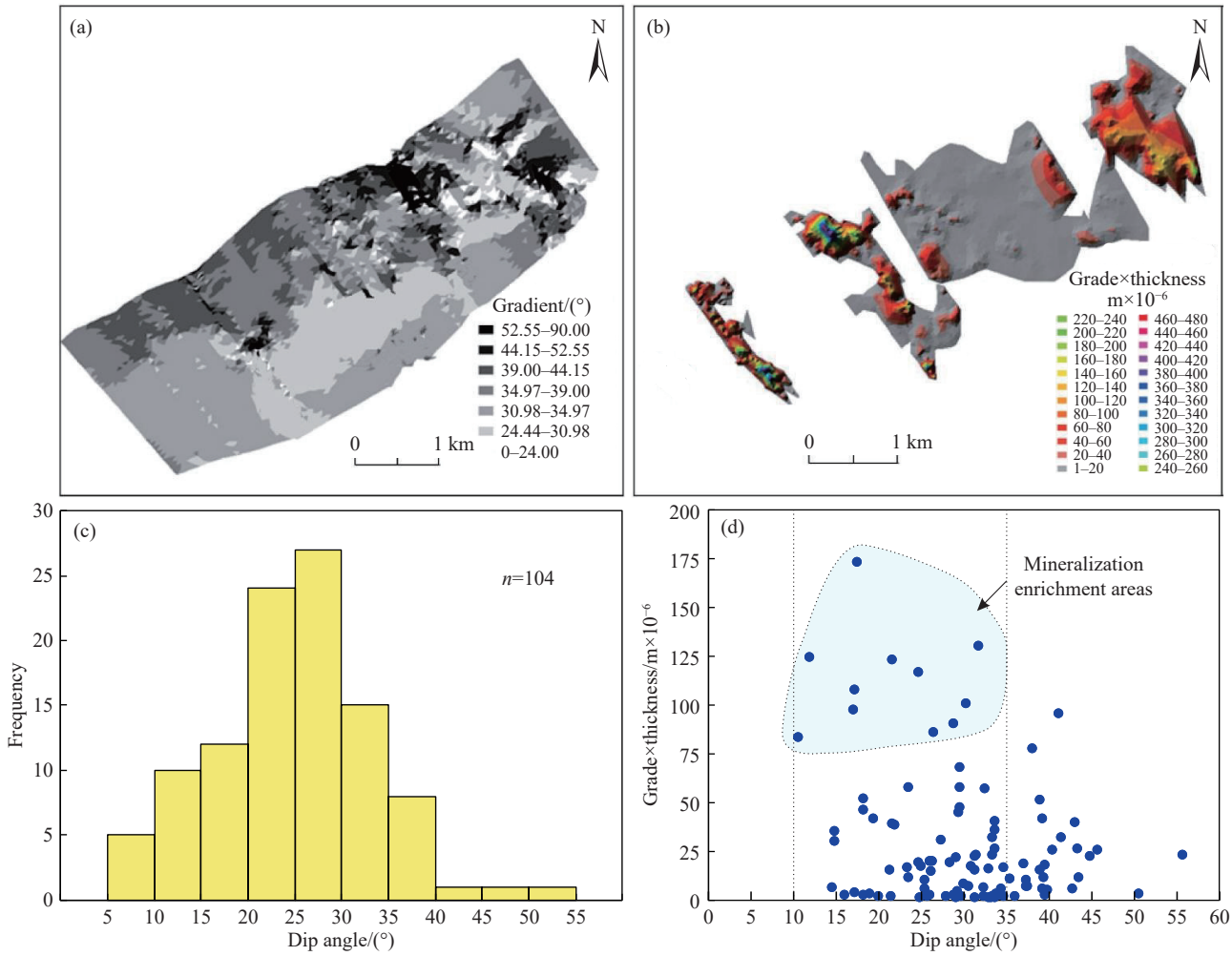

Fig. 7. Diagrams showing the relationships between the fault dip angle, the mineralization enrichment areas of primary orebodies, and the fault dip direction in the Taishang-Shuiwangzhuang gold deposit. a–Three-dimensional map showing the slope of the ore-controlling fault (modified from Wang YQ et al., 2022a); b–three-dimensional map showing the distribution of the thickness×gold grade of priamry orebodies (modified from Wang YQ et al., 2022b); c–histogram showing the ore-controlling fault's dip angle; d–scatter plot showing the thickness × gold grade of orebodies *vs.* ore-controlling fault's dip angle.

well as the Sanshandao and Jiaojia giant gold deposits.

5.2. Timing of gold mineralization

The metallogenic age of gold deposits within the Jiaodong Peninsula has been limited to 120±2 Ma (Deng J et al., 2020c; Zhang L et al., 2020). The metallogenic age of the Taishang-Shuiwangzhuang gold deposit has not yet been reported. However, research has indicated that this gold deposit shares the same origin as quartz vein-type gold deposits in the Linglong gold orefield, both derived from the same stage of hydrothermal activity (Guo LN et al., 2019). For the Taishang-Shuiwangzhuang gold deposit, one sample from a gold-bearing pyrite-quartz vein in Damoqujia yielded a sericite ^{40}Ar-^{39}Ar age of 122.3±0.9 Ma (Chai P et al., 2020); two samples from a gold-bearing pyrite-quartz vein in Fushan yielded sericite ^{40}Ar-^{39}Ar ages of 121.1±0.3 Ma, 121.0±0.2 Ma, and 119.8±0.2 Ma (Zhang L et al., 2020); two samples from disseminated beresite ores in Luoshan yielded sericite ^{40}Ar-^{39}Ar ages of 119.4±3.8 Ma and 121.8±3.2 Ma (Zhang L et al., 2020); and one sample from a gold-bearing pyrite-quartz vein in the Linglong No. 50 vein yielded a hydrothermal monazite U-Pb age of 120.0±4.6 Ma (Deng J et al., 2020c). Therefore, it can be inferred that the Taishang-Shuiwangzhuang gold deposit was formed at around 120 Ma.

5.3. Properties and sources of ore-forming fluids

The ore-forming fluids in the Taishang-Shuiwangzhuang gold deposit are proved to be a H_2O-CO_2-NaCl system with medium-low temperatures and medium-low salinity in general (Yang LQ et al., 2016). From early metallogenic stage I to late metallogenic stage IV, inclusions in the deposit shifted from simple to complex and then to simple types, while ore-forming fluids in the deposit gradually evolved from high to medium and then to low temperatures (Table 1; Fig. 8). The ore-forming fluids of the primary metallogenic stages (II and III) exhibit significantly wider salinity ranges than those of the early and late metallogenic stages (I and IV) (Table 1; Fig. 8). The H_2O-CO_2 inclusions and H_2O solution inclusions formed in the primary metallogenic stages were simultaneously trapped in the same fluid inclusion assemblages (Figs. 6b, e),

exhibiting similar total homogenization temperatures (Table 1) but varying final homogeneous phases and salinity values (Fig. 8; H_2O-rich H_2O-CO_2 fluid inclusions exhibit a final homogeneous phase of liquid and high salinity, whereas the CO_2-rich ones display a final homogeneous phase of vapor and low salinity). This result indicates that significant fluid immiscibility occurred in the primary metallogenic stages (Wang ZL et al., 2015; Yang LQ et al., 2016; Guo LN et al., 2017), leading to reduced contents of volatile constituents, such as CO_2 and H_2S, in fluids and the decomposition of gold-bearing complexes, which induced gold precipitation and mineralization (Phillips GN and Evans KA, 2004; Chi GX and Xue CJ, 2011; Lu HZ, 2011).

Massive studies have been conducted on the characteristics of ore-forming fluids in the Jiaodong gold deposits. However, the source of ore-forming fluids in these deposits remains controversial. Many researchers consider that the ore-forming fluids were dominated by magmatic water in the primary metallogenic stages and were mixed with meteoric water in the late metallogenic stage (Deng J et al., 2015; Li L et al., 2015; Wen BJ et al., 2016; Liu JC et al., 2018; Cai YC et al., 2018). Some researchers hold that the ore-forming fluids might have primarily originated from metamorphic water and were mixed with magmatic water and meteoric water (Yang LQ et al., 2014, 2016, 2017). Some researchers deny the influence of meteoric water on the gold mineralization in the Jiaodong Peninsula, proposing that the H-O isotopic characteristics are attributed to the secondary inclusions formed post-mineralization (Goldfarb RJ and Groves DI, 2015).

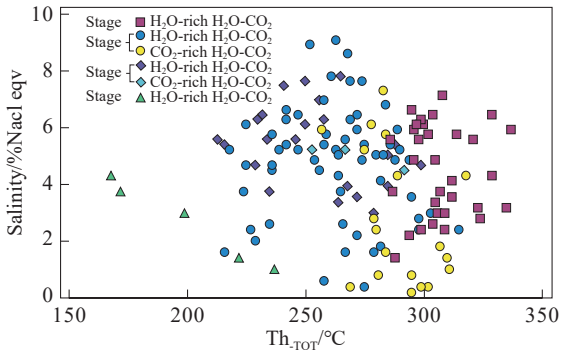

Fig. 8. Plot showing the total homogenization temperature (Th_{-TOT}) *vs.* salinity of fluid inclusions from the Taishang-Shuiwangzhuang gold deposit (data sources provided in Table 1).

The H-O isotopes of the Taishang-Shuiwangzhuang gold deposit do not exhibit significant regular variations from shallow to deep parts, with H-O isotope values generally fluctuating around their averages (Figs. 9a, b). This suggests similar metallogenic environments in the deep and shallow parts. A small portion of the H-O isotope values fell within the zones of primary magmatic water, metamorphic water, and juvenile water, while most of them fell between the zone of Mesozoic meteoric water in the Jiaodong Peninsula and the zone of primary magmatic water, metamorphic water, or juvenile water. The H-O isotopic values of stage I fell within and near the zones of juvenile water and primary magmatic water, while those of stage II/III fell within and near the zone of juvenile water. Furthermore, the H-O isotopic composition gradually drifted toward meteoric water from stage I to stage IV (Fig. 9). Given that the Jiaodong Group exhibits metamorphic ages ranging from approximately 1.8 Ga to 1.7 Ga (Faure M et al., 2003), much earlier than the metallogenic age of the Taishang-Shuiwangzhuang gold deposit, it is unlikely that the ore-forming fluids in the deposit originated from the metamorphic water of the Jiaodong Group. The

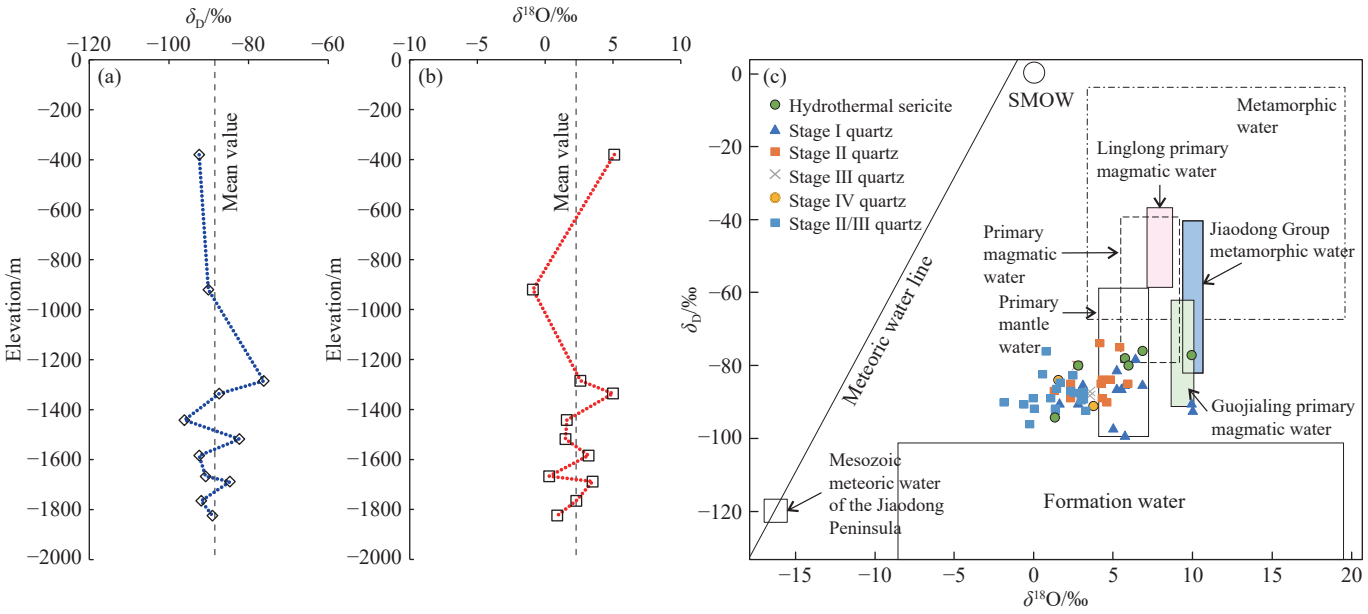

Fig. 9. a–Line graph showing the δD values varying with elevation; b–line graph showing δ^{18}O values varying with elevation; c–δD *vs.* δ^{18}O diagram of ore-forming fluids in the Taishang-Shuiwangzhuang gold deposit (base map from Sheppard SMF, 1986) (references provided in Table 2. Zones for metamorphic water of the Jiaodong Group from Zhang LG et al., 1995b; Linglong and Guojialing primary magmatic water from Zhang LG et al., 1995a and Mao JW et al., 2005; Mesozoic meteoric water of the Jiaodong Peninsula from Zhang LG et al., 1995b).

Early Cretaceous tectono-magmatic activity in the Jiaodong Peninsula and the constant sedimentation in the Jiaolai Basin suggest a lack of significant regional metamorphic activity and the absence of favorable conditions for the formation of metamorphic fluids (Deng J et al., 2023). Furthermore, the ore-forming fluids in the Taishang-Shuiwangzhuang gold deposit demonstrate significant medium-low temperatures and low salinity (<10 wt.% NaCl eqv), greatly distinct from typical high-temperature and high-salinity magmatic fluids (Chen YJ et al., 2007; Yang LQ et al., 2016). Hence, the fluids in the early metallogenic stage might originate from the mantle, with meteoric water gradually involved in the late metallogenic stage. Based on the characteristics of fluid inclusions stated above, this study posits that the ore-forming fluids in the Taishang-Shuiwangzhuang gold deposit were mantle-derived fluids. Specifically, the asthenospheric upwelling during mineralization induced the recycling of the lower crustal materials and the partial melting of the enriched mantle, with fluids formed following the degassing of both the mantle and the mafic magmas formed by the partial melting (Deng J et al., 2023).

5.4. Sources of ore-forming minerals

Debates persist about the sources of ore-forming materials in the Jiaodong gold deposits. Researchers holding the opinion of crust-derived ore-forming materials consider that the ore-forming materials in the deposit originate from the Precambrian metamorphic basement and the Late Jurassic Linglong-type granites in the Jiaodong Peninsula or from the Precambrian accretionary metamorphic complexes that were activated and reconstructed during the Mesozoic (Yang LQ et al., 2014). Researchers holding the view of mantle-derived ore-forming materials posit that metals in the deposit originated primarily from the deep mantle-derived magmas in the source area of intermediate-mafic dikes (Tan J et al., 2015; Yuan ZZ et al., 2019). They held that gold was extracted from the enriched mantle extracted during its partial melting, followed by mineralization (Wang ZC et al., 2020). Some researchers believe that the enriched lithospheric mantle of the North China Craton exhibits a reservoir with high gold content after undergoing long-term subduction and metasomatism (Deng J et al., 2020a, 2020b). In recent years, some researchers have proposed that the ore-forming materials in the deposit are related to the dehydration and desulfurization of the subducted Paleo-Pacific Plate, along with the devolatilization of enriched mantle wedges (Deng J et al., 2015; Yang LQ et al., 2016; Liu XF et al., 2018; Wei YJ et al., 2019; Zhang L et al., 2020).

The S isotopes of the Taishang-Shuiwangzhuang gold deposit also do not display significant regular changes from shallow to deep parts, with S isotope values fluctuating around their averages (Fig. 10a). These isotopes exhibit concentrated $\delta^{34}S_{CDT}$ values and a positive deviation from meteorite sulfur, indicating a high homogenization of S (Fig. 10c). The $\delta^{34}S_{CDT}$ values of the gold deposit largely overlap with those of the Jiaodong Group, the Linglong-, Guojialing-, and Aishan-type granites, and intermediate-mafic dikes (Fig. 10b), suggesting closely related origins. The average $\delta^{34}S_{CDT}$ value of the gold deposit is higher than that of the Jiaodong Group and Early Cretaceous mafic dikes, which contain high proportions of mantle components, lower than that of the crust-derived Jingshan Group, and close to that of the

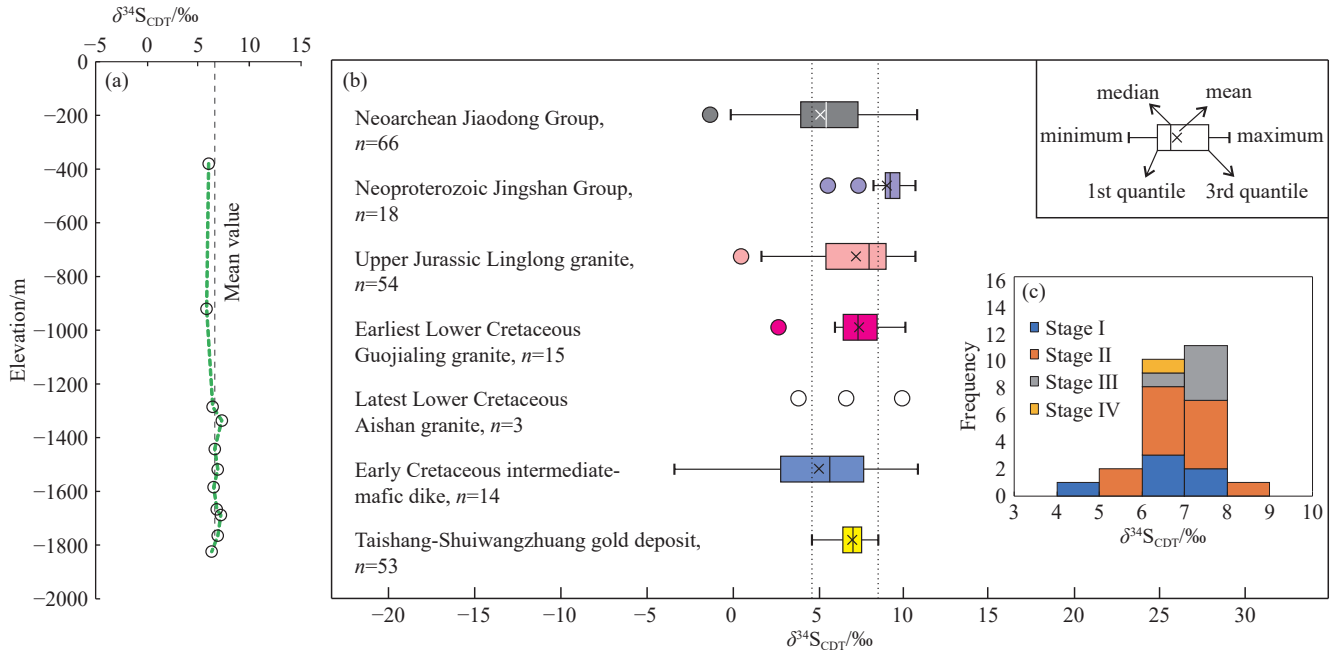

Fig. 10. a–Line diagram showing sulfur isotopic composition varying with elevation; b–sulfur isotopic histogram of the Taishang-Shuiwangzhuang gold deposit; c–comparison of sulfur isotopic compositions between Taishang-Shuiwangzhuang gold deposit, Jiaodong Group, Jingshan Group, Mesozoic magmatic rocks, and intermediate-mafic dikes (data from Yang LQ et al., 2016; Yuan ZZ et al., 2019; Li ZL and Yang MZ, 1993; Mao JW et al., 2005; Hou ML et al., 2006; Chen YM et al., 2016; Li J et al., 2021).

Linglong-type granites formed primarily by crustal remelting and the Guojialing-type granites with an origin of crust-mantle mixing (Hou ML et al., 2007; Wang ZL et al., 2014). These results indicate that the S source in the Taishang-Shuiwangzhuang gold deposit has the characteristics of crust-mantle interactions.

As shown in the $^{207}Pb/^{204}Pb$ *vs.* $^{206}Pb/^{204}Pb$ discriminant diagram of the tectonic environment (Fig. 11), the Pb isotope values of the Taishang-Shuiwangzhuang gold deposit all fell between the evolution curves of the mantle and the upper crust, demonstrating a linear distribution trend. In contrast, the Pb isotope values of the Jiaodong Group fell between or near the evolution curves of the mantle and lower crust, those of the Linglong- and Luanjiahe-type granites fell near the mantle evolution curve and between the evolution curves of the mantle and lower crust, and those of the Guojialing-type granites generally fell between or near the mantle and orogenic evolution curves. All these results indicate the characteristics of mixed crust- and mantle-derived Pb. The Pb isotope values of the ores in the Taishang-Shuiwangzhuang gold deposit largely overlapped with those of the main geological bodies in the Jiaodong Peninsula, indicating that ores share the material sources with and inheriting properties from their surrounding rocks (i.e., the Linglong- and Luanjiahe-type granites, and the Jiaodong Group).

Compared to its ore-hosting rocks, the Taishang-Shuiwangzhuang gold deposit exhibits similar S and Pb isotopic characteristics and more concentrated $\delta^{34}S_{CDT}$ values. This result indicates that the ore-forming materials in the deposit originated primarily from its ore-hosting rocks. The Jiaodong Peninsula underwent intense crust-mantle interactions during the Early Cretaceous. Consequently, the ore-hosting rocks in the peninsula are dominated by crust-derived materials, mixed with substantial mantle-derived materials. Therefore, this study posits that the ore-forming materials in the Taishang-Shuiwangzhuang gold deposit are dominated by crust-derived materials, along with small quantities of mantle-derived materials.

5.5. Metallogenic process and genesis

The Taishang-Shuiwangzhuang gold deposit occurs in the Zhaoping fault zone, whose hanging wall is composed primarily of Late Jurassic Luanjiahe-type granites and Precambrian metamorphic rocks and footwall consists of Late Jurassic Linglong-type granites. This deposit hosts many intermediate-mafic dikes, with Early Cretaceous Guojialing-type granites (such as Guojialing and Congjia plutons) identified near the mining area. These geological bodies and the fault structure are intimately linked to gold mineralization. Studies indicate that the Linglong- and Guojialing-type granites resulted from the partial melting of the paleocrust, while the Weideshan-type granites were formed by the partial melting of the juvenile lower crust (Wang B et al., 2021, 2023). The widespread intermediate-mafic dikes in the deposit signify mantle-derived magmatism. These results indicate that gold mineralization occurred during the transition from ancient to juvenile lower crust and crust-mantle interactions. As shown by the thermochronological results of granites (Charles N et al., 2013), the Linglong-type granites were approximately 800°C when they were formed at 160 Ma, slowly cooling to approximately 450±50°C at approximately 143 Ma; the Guojialing-type granites cooled at a rate of 100°C/Ma from 130–126 Ma to 124 Ma; and the Weideshan-type granites experienced a more rapid cooling process after being formed, rapidly cooling to approximately 350±50°C from 122 Ma to 118 Ma. In contrast, these granites cooled at a rate of above 30°C/Ma from 117 Ma to 110 Ma (Wu L et al., 2018). A thermochronological study of Jiaodong gold deposits post-mineralization indicates that these deposits

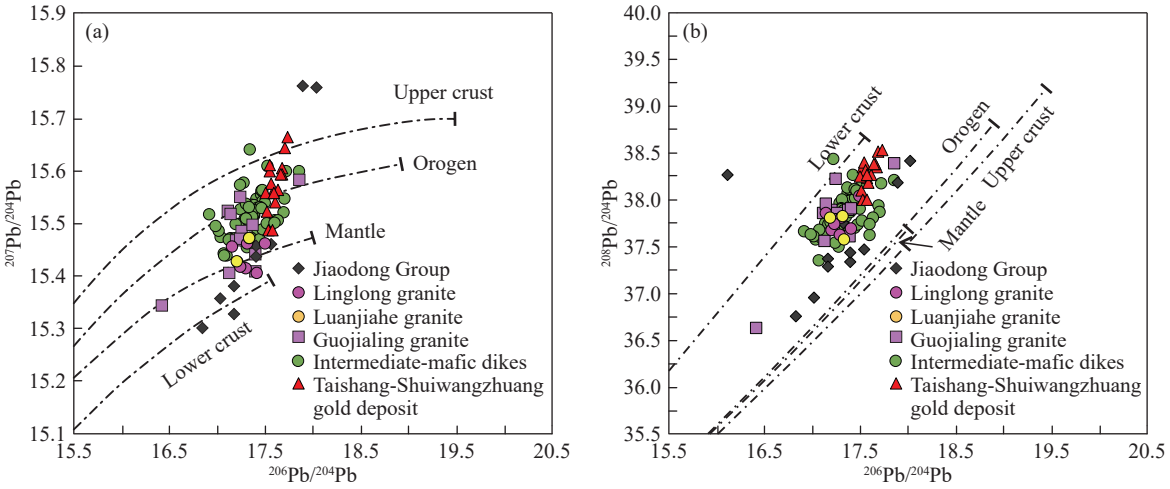

Fig. 11. Lead isotopic compositions of the Taishang-Shuiwangzhuang gold deposit. a–$^{207}Pb/^{204}Pb$ *vs.* $^{206}Pb/^{204}Pb$; b–$^{208}Pb/^{204}Pb$ *vs.* $^{206}Pb/^{204}Pb$ (base map from Zartman RE and Doe BR, 1981) (data sources: Lead isotopic data of the Jiaodong Group from Yang SW, 1986; Li ZL and Yang MZ, 1993; Yuan ZZ et al., 2019; lead isotopic data of Linglong-type granites from Mao JW et al., 2005; lead isotopic data of Luanjiahe-type granites from Li ZL and Yang MZ, 1993; lead isotopic data of Guojialing-type granites from Chen ZS et al., 1994; Ma ZD, 1988; Li ZL and Yang MZ, 1993; Guan K et al., 1997; lead isotopic data of intermediate-basic dikes from Tan J et al., 2012; Cai YC et al., 2013; Ma L et al., 2014; Liu XF et al., 2018).

have experienced a very slow cooling and uplifting process since approximately 95 Ma, with a cooling rate of 0.4–2.4°C/Ma (Zhang QB et al., 2022). Therefore, the gold mineralization of the Taishang-Shuiwangzhuang gold deposit was accompanied by rapid crustal uplifting and cooling.

Based on the aforementioned geological process characteristics related to gold mineralization, this study identified the Taishang-Shuiwangzhuang gold deposit as a typical Jiaodong-type gold deposit (Yang LQ et al., 2014; Deng J et al., 2023), proposing that its formation is associated with crust-mantle interactions, the transformation of the lower crust's properties, and rapid crustal uplift. During the Late Jurassic, the post-collision and compression of the North China and Yangtze plates, as well as the crustal thickening caused by the subduction of the Paleo-Pacific Plate or the Izanagi Plate toward the Asian Continent, led to the remelting of the large-scale continental crust in the Jiaodong Peninsula. As a result, Linglong-type granites were formed (Zhang YQ et al., 2007). During the Early Cretaceous, the subduction and retreat of the Paleo-Pacific Plate destroyed the ancient North China Craton (Zhu RX et al., 2011) and led to the intensive thinning of the lithosphere and the crust, the upwelling of the asthenosphere, and intense crust-mantle material exchange. The partial melting of the enriched lithospheric mantle produced mafic magmas, which were then underplated under the paleo or juvenile crust, inducing the partial melting of rocks at the crust bottom (Qiu LG et al., 2008). The mantle-derived mafic magmas subjected to upward intrusion differentiated, forming lamprophyres and other dark dikes. In contrast, different degrees of mixing, crystallization, and differentiation of mantle- and crust-derived magmas led to the formation of Guojialing, Weideshan, and Laoshan-type granites (Wang B et al., 2023). The crust-mantle interactions, intense magmatism, and material exchange induced by the transformation from the ancient to juvenile lower crust during the Early Cretaceous provided abundant fluids and material sources for gold mineralization. The large-scale magmatism during this period was accompanied by the rapid uplift of intrusions and the crust, along with strong extensional tectonism. Rapid magmatic uplift strongly jacked up shallow surrounding rocks, leading to the formation of detachment faults along the interface between Linglong-type granites and Luanjiahe-type granites or the Precambrian metamorphic rocks. This created favorable spaces for the accumulation and mineralization of ore-forming fluids (Fig. 12). Moreover, the rapid uplift caused sharp decreases in fluid temperature and pressure, resulting in immiscibility (phase separation) or boiling. Consequently, substantial fluid components such as CO_2, and H_2S escaped, leading to elevated pH of the fluid system. Concurrently, fluids containing metal elements like Fe and Cu reacted with those containing S, yielding sulfides such as pyrites and chalcopyrite. Furthermore, the escape and consumption of components such as CO_2 and H_2S reduced the stability of gold-bearing complexes in the fluids. Finally, gold, in the form of native gold and electrum, was precipitated and mineralized along with metal sulfides, such as pyrites, in parts subjected to pressure fluctuations—the steep-to-gentle transition parts of detachment faults.

6. Conclusions

(i) The Taishang-Shuiwangzhuang gold deposit is a giant gold deposit with gold resources of over 700 t. The primary orebodies in the deposit exhibit branching and combination, expansion and contraction, and pinch-out and reoccurrence, with deep and shallow orebodies separated by weak mineralization or ore-free intervals. Orebodies in the deposit

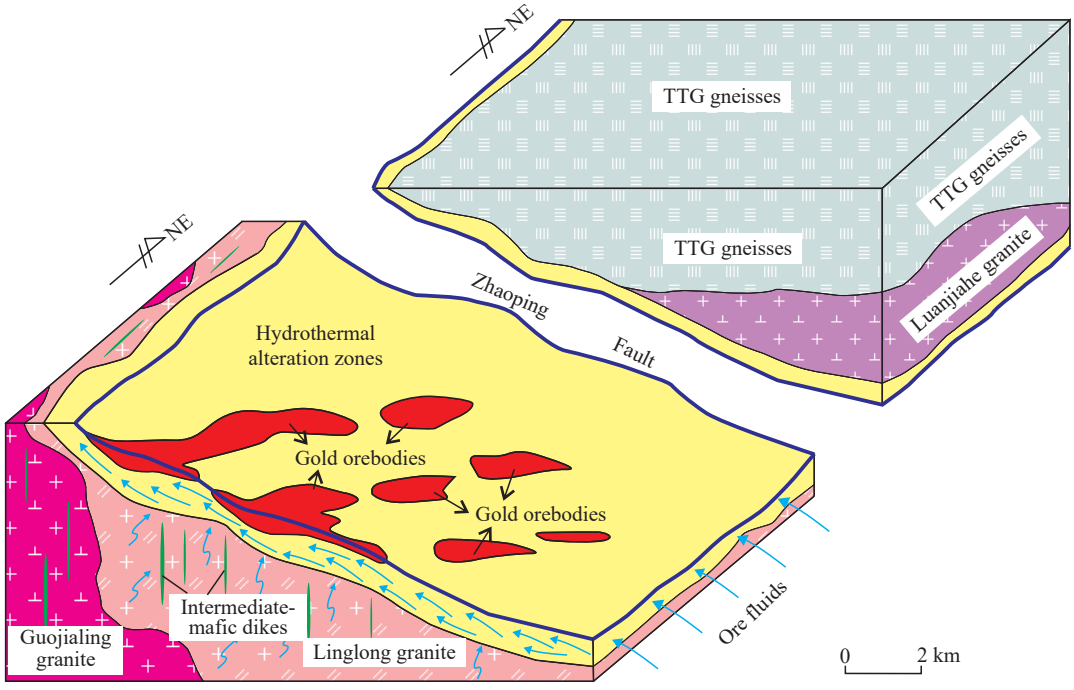

Fig. 12. Schematic diagrams illustrating ore genesis of the Taishang-Shuiwangzhuang gold deposit.

pitch to NEE and plunge toward NEE. The ore-controlling Zhaoping fault exhibits wavy fluctuations, with its dip angle featuring three sections of high-to-low transitions along its plunge direction. The gold mineralization enrichment areas are primarily distributed in the steep-to-gentle transition parts of the Zhaoyuan fault and relatively gentle steps.

(ii) The ore-forming fluids in the Taishang-Shuiwangzhuang gold deposit are identified as a H_2O-CO_2-NaCl hydrothermal system with medium-low temperature and medium-low salinity. These fluids evolved from high to medium and then to low temperatures, with fluid immiscibility occurring in primary metallogenic stages II and III. The H-O isotopic characteristics indicate that the ore-forming fluids of the deposit might have originated from fluids generated following the degassing of both the mantle and the basic magmas formed by partial melting and were mixed with meteoric water in the late stage. The S and Pb isotopic characteristics suggest that the ore-forming materials of the deposit are dominated by crust-derived materials, along with small quantities of mantle-derived materials.

(iii) The Taishang-Shuiwangzhuang gold deposit is proved to be a typical Jiaodong-type gold deposit. The intense crust-mantle interactions, large-scale magmatism, and material exchange induced by the transformation from the ancient to juvenile lower crust during the Early Cretaceous provided abundant fluids and material sources for mineralization. Furthermore, the detachment faults, along with variations in temperature and pressure, formed by rapid magmatic uplift and extensional tectonism created favorable spaces and gold unloading conditions for fluid accumulation and gold precipitation and mineralization.

CRediT authorship contribution statement

Zheng-jiang Ding, Zhong-yi Bao and Xiang-dong Liu conceived and designed the ideas. Xiang-dong Liu and Chun-ming Yan prepared the manuscript. Jia-meng Fan and Tian-ci Xie drew all the figures. Xiang-dong Liu, Chun-ming Yan and Hao-cheng Yu participated in field investigation. Xiang-dong Liu, Tian-ci Xie, and Zhi-ning Liu performed the data processing. Xiang-dong Liu and Hao-cheng Yu reviewed and edited the draft. All authors have read and agreed to the published version of the manuscript.

Declaration of competing interest

The authors declare no conflicts of interest.

Acknowledgment

Professors Li-qiang Yang and Kun-feng Qiu reviewed the entire manuscript and proposed valuable comments. The authors hereby would like to extend their sincere gratitude to them. This paper was financially supported by the National Key Research and Development Program of China (Grant No. 2023YFC2906900), Key Research and Development Program of Shandong Province (Grant No. 2023CXGC011001), The Taishan Scholars Talent Project (TSTP 20240847), The Open Project of Technology Innovation Center for Deep Gold Resources Exploration and Mining, Ministry of Natural Resources(Grant No. SDK202211, SDK202214) and Science and Technology Project of Shandong Bureau of Geology and Mineral Exploration and Development (Grant No. KY202208)

References

Ames L, Zhou GZ, Xiong BC. 1996. Geochronology and isotopic character of ultrahigh-pressure metamorphism with implications for collision of the Sino-Korean and Yangtze cratons, Central China. Tectonics, 15(2), 472–489. doi: 10.1029/95tc02552.

Bao ZY, Sun ZQ, Liu GD, Li S, Fan JM. 2014. Geological characteristics and prospecting direction of deposits in Shuiwangzhuang area in potouqing fault. Shandong Land and Resources, 30(2), 29–33 (in Chinese with English abstract).

Cai YC, Fan HR, Santosh M, Hu FF, Yang KF, Li XH. 2018. Decratonic gold mineralization: Evidence from the Shangzhuang gold deposit, eastern North China Craton. Gondwana Research, 54, 1–22. doi: 10.1016/j.gr.2017.09.009.

Cai YC, Fan HR, Santosh M, Liu X, Hu FF, Yang KF, Lan TG, Yang YH, Liu YS. 2013. Evolution of the lithospheric mantle beneath the southeastern North China Craton: Constraints from mafic dikes in the Jiaobei terrain. Gondwana Research, 24(2), 601–621. doi: 10.1016/j.gr.2012.11.013.

Chai P, Zhang HR, Hou ZQ, Zhang ZY. 2020. Geochronological framework of the damoqujia gold deposit, Jiaodong Peninsula, China: Implications for the timing and geologic setting of gold mineralization. Geological Journal, 55(1), 596–613. doi: 10.1002/gj.3428.

Charles N, Augier R, Gumiaux C, Monié P, Chen Y, Faure M, Zhu RX. 2013. Timing, duration and role of magmatism in wide rift systems: Insights from the Jiaodong Peninsula (China, East Asia). Gondwana Research, 24(1), 412–428. doi: 10.1016/j.gr.2012.10.011.

Chen BH, Wang ZL, Li HL, Li JK, Li JL, Wang GQ. 2014. Evolution of ore fluid of the Taishang gold deposit Jiaodong: Constraints on REE and trace element component of auriferous pyrite. Acta Petrologica Sinica, 30(9), 2518–2532 (in Chinese with English abstract).

Chen JF, Xie Z, Li HM, Zhang XD, Zhou TX, Park YS, Ahn KS, Chen DG, Zhang X. 2003. U-Pb zircon ages for a collision-related K-rich complex at Shidao in the Sulu ultrahigh pressure terrane, China. Geochemical Journal, 37(1), 35–46. doi: 10.2343/geochemj.37.35.

Chen JZ, Jiang N. 2011. Petrogenesis of the Late-Triassic alkaline magmatism in the Jiaodong area: Evidence from U-Pb age, Hf-O isotopes of zircons. Acta Petrologica Sinica, 27(12), 3557–3574 (in Chinese with English abstract).

Chen YJ, Ni P, Fan HR, Pirajno F, Lai Y, Su WC, Zhang H. 2007. Diagnostic fluid inclusions of different types hydrothermal gold deposits. Acta Petrologica Sinica, 23(9), 2085–2108 (in Chinese with English abstract).

Chen YM, Fan HR, Cui L. 2016. Large-Scale Gold Mineralization and Genetic Model of Northwestern Jiaodong. Beijing, Geological Publishing House, 205–217 (in Chinese).

Chen ZS, Zhang LG, Liu JX, Wang BC, Xu JF, Zheng WS. 1994. A study on lead isotope geochemical backgrounds of geological bodies in Jiaodong region. Contributions to Geology and Mineral Resources Research, 9(1), 65–78 (in Chinese with English abstract).

Chi GX, Xue CJ. 2011. Abundance of CO_2-rich fluid inclusions in a sedimentary basin-hosted Cu deposit at Jinman, Yunnan, China: Implications for mineralization environment and classification of the deposit. Mineralium Deposita, 46(4), 365–380. doi: 10.1007/s00126-011-0337-8.

Clayton RN, O'Neil JR, Mayeda TK. 1972. Oxygen isotope exchange between quartz and water. Journal of Geophysical Research, 77(17), 3057–3067. doi: 10.1029/jb077i017p03057.

Deng J, Liu XF, Wang QF, Dilek Y, Liang YY. 2017. Isotopic characterization and petrogenetic modeling of Early Cretaceous mafic diking —Lithospheric extension in the North China Craton, eastern Asia. GSA Bulletin, 129(11–12), 1379–1407. doi: 10.1130/b31609.1.

Deng J, Liu XF, Wang QF, Pan RG. 2015. Origin of the Jiaodong-type xinli gold deposit, Jiaodong Peninsula, China: Constraints from fluid inclusion and C–D–O–S–Sr isotope compositions. Ore Geology Reviews, 65, 674–686. doi: 10.1016/j.oregeorev.2014.04.018.

Deng J, Qiu KF, Wang QF, Goldfarb R, Yang LQ, Zi JW, Geng JZ, Ma Y. 2020a. *In situ* dating of hydrothermal monazite and implications for the geodynamic controls on ore formation in the Jiaodong gold province, Eastern China. Economic Geology, 115(3), 671–685. doi: 10.5382/econgeo.4711.

Deng J, Wang QF, Santosh M, Liu XF, Liang YY, Yang LQ, Zhao R, Yang L. 2020b. Remobilization of metasomatized mantle lithosphere: A new model for the Jiaodong gold province, Eastern China. Mineralium Deposita, 55(2), 257–274. doi: 10.1007/s00126-019-00925-0.

Deng J, Qiu KF, Wang QF, Goldfarb R, Yang LQ, Zi JW, Geng JZ, Ma Y. 2023. *In situ* dating of hydrothermal monazite and implications for the geodynamic controls on ore formation in the Jiaodong gold province, Eastern China. Economic Geology, 66(10), 2287–2310 (in Chinese with English abstract). doi: 10.1007/s11430-022-1136-4.

Deng J, Wang QF. 2016. Gold mineralization in China: Metallogenic provinces, deposit types and tectonic framework. Gondwana Research, 36, 219–274. doi: 10.1016/j.gr.2015.10.003.

Deng J, Yang LQ, Groves DI, Zhang L, Qiu KF, Wang QF. 2020c. An integrated mineral system model for the gold deposits of the giant Jiaodong province, Eastern China. Earth-Science Reviews, 208, 103274. doi: 10.1016/j.earscirev.2020.103274.

Deng J, Yang LQ, Li RH, Groves DI, Santosh M, Wang ZL, Sai SX, Wang SR. 2019. Regional structural control on the distribution of world-class gold deposits: An overview from the Giant Jiaodong Gold Province, China. Geological Journal, 54(1), 378–391. doi: 10.1002/gj.3186.

Fan HR, Lan TG, Li XH, Santosh M, Yang KF, Hu FF, Feng K, Hu HL, Peng HW, Zhang YW. 2021. Conditions and processes leading to large-scale gold deposition in the Jiaodong province, eastern China. Science China Earth Sciences, 64(9), 1504–1523 (in Chinese with English abstract). doi: 10.1007/s11430-020-9789-2.

Faure M, Lin W, Monié P, Le Breton N, Poussineau S, Panis D, Deloule E. 2003. Exhumation tectonics of the ultrahigh-pressure metamorphic rocks in the Qinling orogen in East China: New petrological-structural-radiometric insights from the Shandong Peninsula. Tectonics, 22(3), 1018. doi: 10.1029/2002tc001450.

Gao TS, Chen JF, Xie Z, Yan J, Qian H. 2004. Geochemistry of Triassic igneous complex at Shidao in the Sulu UHP metamorphic belt. Acta Petrologica Sinica, 20(5), 36–49 (in Chinese with English abstract).

Geng K, Wang RJ, Li HK, Liang TT, Zhang YB. 2016. Zircon SHRIMP U-Pb geochronology of Congjia granodiorite from northwest Jiaodong area. Acta Geoscientica Sinica, 37(1), 90–100 (in Chinese with English abstract). doi: 10.3975/cagsb.2016.01.09.

Goldfarb RJ, Groves DI. 2015. Orogenic gold: Common or evolving fluid and metal sources through time. Lithos, 233, 2–26. doi: 10.1016/j.lithos.2015.07.011.

Goss SC, Wilde SA, Wu FY, Yang JH. 2010. The age, isotopic signature and significance of the youngest Mesozoic granitoids in the Jiaodong Terrane, Shandong Province, North China Craton. Lithos, 120(3–4), 309–326. doi: 10.1016/j.lithos.2010.08.019.

Groves DI, Santosh M, Goldfarb RJ, Zhang L. 2018. Structural geometry of orogenic gold deposits: Implications for exploration of world-class and giant deposits. Geoscience Frontiers, 9(4), 1163–1177. doi: 10.1016/j.gsf.2018.01.006.

Guan K, Luo ZK, Miao LC, Huang JZ. 1997. Petrochemical and geochemical characteristics of guojialing suite granite in zhaoye district and the genetic relation of gold mineralization to the granite. Conributions to Geology and Mineral Resources Research, 12(4), 1–8 (in Chinese with English abstract).

Guo JH, Chen FK, Zhang XM, Siebel W, Zhai MG. 2005. Evolution of syn- to post-collisional magmatism from north Sulu UHP belt, eastern China: Zircon U-Pb geochronology. Acta Petrologica Sinica, 21(4), 1281–1301 (in Chinese with English abstract). doi: 10.3969/j.issn.1000-0569.2005.04.025.

Guo LN, Goldfarb RJ, Wang ZL, Li RH, Chen BH, Li JL. 2017. A comparison of Jiaojia- and Linglong-type gold deposit ore-forming fluids: Do they differ? Ore Geology Reviews, 88, 511–533. doi: 10.1016/j.oregeorev.2016.12.003.

Guo LN, Huang CM, Zhang L, Chen BH, Li RH, Liu Y. 2019. Source of ore-forming fluids in the Luoshan gold deposit, Jiaodong: Constrains from REE and trace element features of auriferous pyrite in the altered-rock type and auriferous quartz vein type ores. Geoscience, 33(1), 121–136 (in Chinese with English abstract). doi: 10.19657/j.geoscience.1000-8527.2019.01.12.

Guo LN. 2016. Metallogenic mechanism of the Jiaodong-type gold deposit, Shandong Province, China. Beijing, China University of Geosciences (Beijing), Ph. D. Dissertation, 1–192 (in Chinese with English abstract).

Hou ML, Jiang SY, Jiang YH, Ling HF. 2006. S-Pb isotope geochemistry and Rb-Sr geochronology of the Penglai gold field in the eastern Shangdong province. Acta Petrologica Sinica, 22(10), 2525–2533 (in Chinese with English abstract).

Hou ML, Jiang YH, Jiang SY, Ling HF, Zhao KD. 2007. Contrasting origins of late Mesozoic adakitic granitoids from the northwestern Jiaodong Peninsula, East China: Implications for crustal thickening to delamination. Geological Magazine, 144(4), 619–631. doi: 10.1017/s0016756807003494.

Jiang N, Chen JZ, Guo JH, Chang GH. 2012. *In situ* zircon U–Pb, oxygen and hafnium isotopic compositions of Jurassic granites from the North China Craton: Evidence for Triassic subduction of continental crust and subsequent metamorphism-related ^{18}O depletion. Lithos, 142–143, 84–94. doi: 10.1016/j.lithos.2012.02.018.

Li J, Zhang LP, Song MC, Liang JL, Li SY, Song YX, Bao ZY, Ding ZJ. 2021. Formation mechanism of shuiwangzhuang gold deposit in Jiaodong Peninsula: Constraints from S-H-O isotopes and fluid inclusions. Earth Science, 46(5), 1569–1584 (in Chinese with English abstract). doi: 10.3799/dqkx.2020.358.

Li JL, Zhang YQ, Liu ZQ, Ren FL, Yuan JY. 2007. Sedimentary-subsidence history and tectonic evolution of the Jiaolai basin, Eastern China. Geology in China, 34(2), 240–250 (in Chinese with English abstract).

Li L, Santosh M, Li SR. 2015. The 'Jiaodong type' gold deposits: Characteristics, origin and prospecting. Ore Geology Reviews, 65, 589–611. doi: 10.1016/j.oregeorev.2014.06.021.

Li SJ. 1998. Division and correlation of Jurassic and Cretaceous strata in Shandong. Journal of the University of Petroleum, China, 22(1), 1–4 (in Chinese with English abstract). doi: CNKI:SUN:SYDX.0.1998-01-000.

Li SX, Liu CC, An YH. 2007. Geology of Gold Deposits in Jiaodong. Beijin, Geological Publishing House, 8–290 (in Chinese).

Li ZL, Yang MZ. 1993. The Geology-Geochemistry of Gold Deposits in Jiaodong Region. Tianjin, Tianjin Science and Tecnology Press, 10–64 (in Chinese).

Liu GD, Li J. 2019. Geological characteristics and prospecting criteria of super large scale gold deposit of Zhaoping fault zone at the depth of-2200 m in Jiaodong area. Shandong Land and Resources, 35(1), 1–7 (in Chinese with English abstract). doi: 10.12128/j.issn.1672-6979.2019.01.001.

Liu GD, Song GZ, Bao ZY, Li RX, Wen GJ, Liu JH, Liu CJ, Guo ZF,

Fan JM, Yan CM, Li S. 2019. New breakthrough of deep prospecting in the northern section of the Zhaoping fault zone and the new understanding of fault distribution in the Jiaodong district. Geotectonica et Metallogenia, 43(2), 226–234 (in Chinese with English abstract). doi: 10.16539/j.ddgzyckx.2019.02.003.

Liu GD, Wen GJ, Liu CJ, Bao ZY, Sun ZQ, Fan JM, Li S, Yan CM, Guo ZF. 2017. Discovery, characteristics and prospecting direction of Shuiwangzhuang deep super-large gold deposit in the northern section of Zhaoping fault. Gold Science and Technology, 25(3), 38–45 (in Chinese with English abstract).

Liu JC, Wang JY, Liu Y, Tian JX, Li XZ, Zhang HD. 2017. Ore genesis of the Xiadian gold deposit, Jiaodong Peninsula, East China: Information from fluid inclusions and mineralization. Geological Journal, 53, 77–95. doi: 10.1002/gj.3042.

Liu LS, Liu FL, Ji L, Wang W, Wang F, Cai J, Liu PH. 2018. The polygenetic meta-granitic rocks and their geological significance, within the North Sulu ultrahigh-pressure belt. Acta Petrologica Sinica, 34(6), 1557–1580 (in Chinese with English abstract).

Liu XD, Deng J, Zhang L, Lin SY, Zhou ML, Song YZ, Xu XL, Lian CQ. 2019. Hydrothermal alteration of the Sizhuang gold deposit, northwestern Jiaodong Peninsula, Eastern China. Acta Petrologica Sinica, 35(5), 1551–1565 (in Chinese with English abstract). doi: 10.18654/1000-0569/2019.05.15.

Liu XD, Ding ZJ, Song MC, Zhou ML, Xu SH, Yang ZL, Xie TC, Cui T, Song YX, Gao XK, Li RX, Zhang LL, Zhang QB, Wang SS, Wang B. 2022. Geology and mineralization of the Dayin'gezhuang supergiant gold deposit (180 t) in the Jiaodong Peninsula, China: A review. China Geology, 5, 1–26. doi: 10.31035/cg2022058.

Liu XD, Zhou ML, Xu SH, Yin ZK, Xu ZH, Liu GD, Fan JM. 2022. Prospecting prediction and verification at a depth of 3000 m in the Shuiwangzhuang gold deposit, northwestern Jiaodong Peninsula, Eastern China. Geological Bulletin of China, 41(6), 946–957 (in Chinese with English abstract). doi: 10.12097/j.issn.1671-2552.2022.06.003.

Liu XF, Deng J, Liang YY, Wang QF, Pan RG, Qin C, Yang Y. 2018. Petrogenesis of Early Cretaceous intermediate-felsic dikes in the Jiaodong Peninsula, south-eastern North China Craton: Constraints from geochronology, geochemistry and Sr-Nd-Pb-Hf isotopes. Gondwana Research, 60, 69–93. doi: 10.1016/j.gr.2018.04.005.

Liu Y, Deng J, Wang ZL, Zhang L, Zhang C, Liu XD, Zheng XL, Wang XD. 2014. Zircon U-Pb age Lu-Hf isotopes and petrogeochemistry of the monzogranites from Xincheng gold deposit northwestern Jiaodong Peninsula China. Acta Petrologica Sinica, 30(9), 2559–2573 (in Chinese with English abstract).

Lu HZ. 2011. Fluids immiscibility and fluid inclusions. Acta Petrologica Sinica, 27(5), 1253–1261 (in Chinese with English abstract).

Ma L, Jiang SY, Dai BZ, Jiang YH, Hou ML, Pu W, Xu B. 2013. Multiple sources for the origin of Late Jurassic Linglong adakitic granite in the Shandong Peninsula, Eastern China: Zircon U–Pb geochronological, geochemical and Sr–Nd–Hf isotopic evidence. Lithos, 162–163, 251–263. doi: 10.1016/j.lithos.2013.01.009.

Ma L, Jiang SY, Hou ML, Dai BZ, Jiang YH, Yang T, Zhao KD, Pu W, Zhu ZY, Xu B. 2014. Geochemistry of Early Cretaceous calc-alkaline lamprophyres in the Jiaodong Peninsula: Implication for lithospheric evolution of the eastern North China Craton. Gondwana Research, 25(2), 859–872. doi: 10.1016/j.gr.2013.05.012.

Ma ZD. 1988. Discussion on characteristic of lead isotope composition of original gold deposits in Sino-Korean paraplatform and relation to some problems. Earth Science, 13(4), 395–402 (in Chinese with English abstract).

Mao JW, Hua RM, Li XB. 1999. A preliminary study of LARGE$_S$CALE metallogenesis and large clusters of mineral deposits. Mineral Deposits, 18(4), 291–299 (in Chinese with English abstract).

Mao JW, Li HM, Wang YT, Zhang CQ, Wang RT. 2005. The relationship between mantle-derived fluid and gold ore-formation in the eastern Shandong Peninsula: Evidences from D-O-C-S isotopes. Acta Geologica Sinica, 79(6), 839–857 (in Chinese with English abstract).

Phillips GN, Evans KA. 2004. Role of CO_2 in the formation of gold deposits. Nature, 429(6994), 860–863. doi: 10.1038/nature02644.

Qiu LG, Ren FL, Cao ZX, Zhang YQ. 2008. Late Mesozoic magmatic activities and their constraints on geotectonics of Jiaodong region. Geotectonica et Metallogenia, 32(1), 117–123 (in Chinese with English abstract). doi: 10.16539/j.ddgzyckx.2008.01.003.

Ren FL, Liu ZQ, Qiu LG, Han LG, Zhang YQ, Cao ZX. 2008. The prototype character of Jiaolai basin in Cretaceous Laiyang period. Acta Sedimentologica Sinica, 26(2), 221–233 (in Chinese with English abstract).

Sheppard SMF. 1986. Characterization and isotopic variations in natural waters. Reviews in Mineralogy & Geochemistry, 16, 165–183

Song MC, Ding ZJ, Liu XD, Li SY, Li J, Dong LL, Wei XF, Bao ZY, Wang B, Zhang QB, Zhang LL, Liu HB, He CY. 2022. Structural controls on the Jiaodong type gold deposits and metallogenic model. Acta Geologica Sinica, 96(5), 1774–1802 (in Chinese with English abstract). doi: 10.19762/j.cnki.dizhixuebao.2022143.

Song MC, Ding ZJ, Zhang JJ, Song YX, Bo JW, Wang YQ, Liu HB, Li SY, Li J, Li RX, Wang B, Liu XD, Zhang LL, Dong LL, Li J, He CY. 2021. Geology and mineralization of the Sanshandao supergiant gold deposit (1200 t) in the Jiaodong Peninsula, China: A review. China Geology, 4(4), 1–34. doi: 10.31035/cg2021070.

Song MC, Lin SY, Yang LQ, Song YX, Ding ZJ, Li J, Li SY, Zhou ML. 2020. Metallogenic model of Jiaodong peninsula gold deposits. Mineral Deposits, 39(2), 215–236 (in Chinese with English abstract). doi: 10.16111/j.0258-7106.2020.02.002.

Song MC, Song YX, Li J, Liu HB, Li J, Dong LL, He CY, Wang RS. 2023. Thermal doming-extension metallogenic system of Jiaodong type gold deposits. Acta Petrologica Sinica, 39(5), 1241–1260 (in Chinese with English abstract). doi: 10.18654/1000-0569/2023.05.02.

Song MC, Wang B, Song YX, Li J, Zheng JF, Li SY, Fan JM, Yang ZL, He CY, Gao MX, Wang YQ, Li RX. 2023. Spatial coupling relationship between faults and gold deposits in the Jiaodong ore concentration area and the effect of thermal doming-extension on mineralisation. Ore Geology Reviews, 153, 105277. doi: 10.1016/j.oregeorev.2022.105277.

Song MC, Yi PH, Xu JX, Cui SX, Shen K, Jiang HL, Yuan WH, Wang HJ. 2012. A step metallogenetic model for gold deposits in the northwestern Shandong Peninsula, China. Science China Earth Sciences, 55(6), 940–948. doi: 10.1007/s11430-012-4366-7.

Tan J, Wei JH, Audétat A, Pettke T. 2012. Source of metals in the Guocheng gold deposit, Jiaodong Peninsula, North China Craton: Link to Early Cretaceous mafic magmatism originating from Paleoproterozoic metasomatized lithospheric mantle. Ore Geology Reviews, 48, 70–87. doi: 10.1016/j.oregeorev.2012.02.008.

Tan J, Wei JH, Li YJ, Fu LB, Li HM, Shi WJ, Tian N. 2015. Origin and geodynamic significance of fault-hosted massive sulfide gold deposits from the Guocheng–Liaoshang metallogenic belt, eastern Jiaodong Peninsula: Rb–Sr dating, and H–O–S–Pb isotopic constraints. Ore Geology Reviews, 65, 687–700. doi: 10.1016/j.oregeorev.2014.06.007.

Wallis S, Enami M, Banno S. 1999. The Sulu UHP terrane: A review of the petrology and structural geology. International Geology Review, 41(10), 906–920. doi: 10.1080/00206819909465178.

Wan D. 2014. Study on Metallogenic Regularities and Metallogenic Prognosis of Gold Deposits in Northern Zhaoping Fracture, Jiaodong Area, Shandong, China. Changchun, Jilin University, Ph. D. Dissertation, 1–200 (in Chinese with English abstract)

Wang B, Song MC, Huo G, Zhou ML, Xu ZH, Jiang L, Song YX, Li J. 2021. Source characteristics and tectonic evolution of Late Mesozoic granites in Jiaodong and their implications for gold mineralization. Acta Petrologica et Mineralogica, 40(2), 288–320 (in Chinese with

English abstract).

Wang B, Zhou JB, Ding ZJ, Wilde SA, Song MC, Zhao TQ, Bao ZY. 2023. Late Mesozoic magmatism and gold metallogeny of the Jiaodong Peninsula, China: A response to the destruction of the North China Craton. Geological Society of America Bulletin, 136(3), 1395–1412. doi: 10.1130/B37057.1.

Wang YQ, Li S, Yang ZL, Liu CJ, Sui XL, Liu XD. 2022. Three-dimensional geological characteristics and fracture-controlling laws of Lingnan-Shuiwangzhuang giant gold deposit in Jiaodong. Geological Bulletin of China, 41(6), 977–985 (in Chinese with English abstract).

Wang YQ, Niu T, Yang ZL, Li RX, Liu TP, Zhang T. 2022. Construction of three-dimensional geological model and spatial distribution law of ore body in Taishang-Shuiwangzhuang section of Zhaoping fault zone. Shandong Land and Resources, 38(7), 12–19 (in Chinese with English abstract). doi: 10.12128/j.issn.1672-6979.2022.07.002.

Wang YW. 1988. Lead isotope composition of gold deposits, north-western Jiaodong Shandong, and its geological significance. Journal of Jilin University (Earth Science Edition), 18(3), 277–286 (in Chinese with English abstract).

Wang ZC, Cheng H, Zong KQ, Geng XL, Liu YS, Yang JH, Wu FY, Becker H, Foley S, Wang CY. 2020. Metasomatized lithospheric mantle for Mesozoic giant gold deposits in the North China Craton. Geology, 48(2), 169–173. doi: 10.1130/g46662.1.

Wang ZL, Yang LQ, Deng J, Santosh M, Zhang HF, Liu Y, Li RH, Huang T, Zheng XL, Zhao H. 2014. Gold-hosting high Ba-Sr granitoids in the Xincheng gold deposit, Jiaodong Peninsula, East China: Petrogenesis and tectonic setting. Journal of Asian Earth Sciences, 95, 274–299. doi: 10.1016/j.jseaes.2014.03.001.

Wang ZL, Yang LQ, Guo LN, Marsh E, Wang JP, Liu Y, Zhang C, Li RH, Zhang L, Zheng XL, Zhao RX. 2015. Fluid immiscibility and gold deposition in the Xincheng deposit, Jiaodong Peninsula, China: A fluid inclusion study. Ore Geology Reviews, 65, 701–717. doi: 10.1016/j.oregeorev.2014.06.006.

Wei YJ, Yang LQ, Feng JQ, Wang H, Lv GY, Li WC, Liu SG. 2019. Ore-fluid evolution of the sizhuang orogenic gold deposit, Jiaodong Peninsula, China. Minerals, 9(3), 190. doi: 10.3390/min9030190.

Wen BJ, Fan HR, Hu FF, Liu X, Yang KF, Sun ZF, Sun ZF. 2016. Fluid evolution and ore genesis of the giant Sanshandao gold deposit, Jiaodong gold province, China: Constrains from geology, fluid inclusions and H-O-S-He-Ar isotopic compositions. Journal of Geochemical Exploration, 171, 96–112. doi: 10.1016/j.gexplo.2016.01.007.

Wu L, Monié P, Wang F, Lin W, Ji WB, Yang LK. 2018. Multi-phase cooling of Early Cretaceous granites on the Jiaodong Peninsula, East China: Evidence from $^{40}Ar/^{39}Ar$ and (U-Th)/He thermochronology. Journal of Asian Earth Sciences, 160, 334–347. doi: 10.1016/j.jseaes.2017.11.014.

Yang LQ, Deng J, Guo LN, Wang ZL, Li XZ, Li JL. 2016. Origin and evolution of ore fluid, and gold-deposition processes at the giant Taishang gold deposit, Jiaodong Peninsula, Eastern China. Ore Geology Reviews, 72, 585–602. doi: 10.1016/j.oregeorev.2015.08.021.

Yang LQ, Deng J, Song MC, Yu XF, Wang ZL, Li RH, Wang SR. 2019. Structure control on formation and localization of giant deposits: An example of Jiaodong gold deposits in China. Geotectonica et Metallogenia, 43(3), 431–446 (in Chinese with English abstract). doi: 10.16539/j.ddgzyckx.2019.03.005.

Yang LQ, Deng J, Wang ZL, Zhang L, Guo LN, Song MC, Zheng XL. 2014. Mesozoic gold metallogenic system of the Jiaodong gold province, Eastern China. Acta Petrologica Sinica, 30(9), 2447–2467 (in Chinese with English abstract).

Yang LQ, Dilek Y, Wang ZL, Weinberg RF, Liu Y. 2018. Late Jurassic, high Ba–Sr linglong granites in the Jiaodong Peninsula, East China: Lower crustal melting products in the eastern North China Craton. Geological Magazine, 155(5), 1040–1062. doi: 10.1017/s0016756816001230.

Yang LQ, Guo LN, Wang ZL, Zhao RX, Song MC, Zheng XL. 2017. Timing and mechanism of gold mineralization at the Wang'ershan gold deposit, Jiaodong Peninsula, Eastern China. Ore Geology Reviews, 88, 491–510. doi: 10.1016/j.oregeorev.2016.06.027.

Yang SW. 1986. A discussion on the Jiaodong group strata, the source-bed of gold and the stratabound features of gold ore deposits in northwest part of Jiaodong peninsula. Contributions to Geology and Mineral Resources Research, 1(3), 39–49 (in Chinese with English abstract).

Yuan ZZ, Li ZK, Zhao XF, Sun HS, Qiu HN, Li JW. 2019. New constraints on the genesis of the giant Dayingezhuang gold (silver) deposit in the Jiaodong district, North China Craton. Ore Geology Reviews, 112, 103038. doi: 10.1016/j.oregeorev.2019.103038.

Zartman RE, Doe BR. 1981. Plumbotectonics —The model. Tectonophysics, 75(1–2), 135–162. doi: 10.1016/0040-1951(81)90213-4.

Zhai MG, Fan HR, Yang JH, Miao LC. 2004. Large-scale cluster of gold deposits in east Shandong: Anorogenic metallogenesis. Earth Science Frontiers, 11(1), 85–98 (in Chinese with English abstract).

Zhang J, Zhao ZF, Zheng YF, Dai MN. 2010. Postcollisional magmatism: Geochemical constraints on the petrogenesis of Mesozoic granitoids in the Sulu orogen, China. Lithos, 119(3–4), 512–536. doi: 10.1016/j.lithos.2010.08.005.

Zhang L, Weinberg RF, Yang LQ, Groves DI, Sai SX, Matchan E, Phillips D, Kohn BP, Miggins DP, Liu Y, Deng J. 2020. Mesozoic orogenic gold mineralization in the Jiaodong Peninsula, China: A focused event at 120 ± 2 ma during cooling of pregold granite intrusions. Economic Geology, 115(2), 415–441. doi: 10.5382/econgeo.4716.

Zhang LG, Chen ZS, Liu JX, Yu GX, Wang BC, Xu JF, Zheng WS. 1995a. Water-rock exchange in the Jiaojia style gold deposit-hydrogen and oxygen isotopic study of altered rocks. Mineral Deposits, 14(3), 261–272 (in Chinese with English abstract)

Zhang LG, Chen ZS, Liu JX, Yu GX, Wang KF, Wang BC, Xu JF, Zheng WS, Li DY, Li H, Hou DY. 1995b. Two-Stage Water-Rock Isotope Exchange Theory and Its Exploration Application. Beijing, Geological Publishing House, 1–220 (in Chinese)

Zhang QB, Song MC, Ding ZJ, Guo ML, Zhou ML, Dai CG, Huo G, Zhang P. 2022. Exhumation history and preservation of the Jiaojia giant gold deposit, Jiaodong Peninsula. Science China Earth Sciences, 65(6), 1161–1177. doi: 10.1007/s11430-021-9887-1.

Zhang YQ, Dong SW, Zhao Y, Zhang T. 2007. Jurassic tectonics of North China: A synthetic view. Acta Geologica Sinica, 81(11), 1462–1480 (in Chinese with English abstract). doi: 10.3321/j.issn:0001-5717.2007.11.002.

Zhao LQ, Deng J, Yuan HT, Li XY. 2008. Short wavelength infrared spectral analysis of alteration zone in the Taishang gold deposit. Geology and Exploration, 44(5), 58–63 (in Chinese with English abstract)

Zhou FY, Li ZL. 1991. A study on inclusions in minerals of Taishang gold deposit, eastern Shandong province. Acta Mineralogica Sinica, 11(4), 403–412 (in Chinese with English abstract)

Zhou FY, Li ZL. 1994. Experimental study on the simulation of the emplacement mechanism of the Taishang gold deposit, Jiaodong, Shandong province. Geological Review, 40(5), 456–465 (in Chinese with English abstract)

Zhu RX, Chen L, Wu FY, Liu JL. 2011. Timing, scale and mechanism of the destruction of the North China Craton. Science China Earth Sciences, 54(6), 789–797. doi: 10.1007/s11430-011-4203-4.